CHARGE PRONG MULTIPLICITY DISTRIBUTIONS IN PROTON-PROTON COLLISIONS AT 28.5 GeV/c

by

Thomas S. Clifford

Dissertation submitted to the Graduate Faculty of the
Virginia Polytechnic Institute and State University
in partial fulfillment of the requirements for the degree of

DOCTOR OF PHILOSOPHY

in

Physics

APPROVED:

W. P. Trower, Chairperson

S. P. Almeida

M. C. Li

A. Robeson

R. F. Tipsword

June, 1974

Blacksburg, Virginia

ACKNOWLEDGEMENTS

There are so many people who have helped to provide me with the material, moral and intellectual support which I needed in order to participate in AGS Experiment 396 and prepare this thesis that it is impossible to mention them all individually. The support I received in all three catagories from Frank Turkot and his group at BNL is deeply appreciated.

I am grateful to J.R. Ficenec and my advisor, W.P. Trower, for their help, suggestions, and encouragement in the preparation of this work.

I also wish to acknowledge the encouragement and presence my wife, Marlene, has provided during this whole project.

TABLE OF CONTENTS

LIST OF TABLES

LIST OF FIGURES

CHAPTER I

INTRODUCTION

Particle production in proton-proton interactions have long been a rich source of experimental data. Most recently particle production in p-p final states has stimulated much phenomenological speculation and model building. The traditional instrument used to collect particle production data, the bubble chamber, can only detect processes with large cross sections, $> 10^{-32} cm^2$. Recognizing this we conceived, designed, and recently completed an experiment at the Brookhaven National Laboratory, BNL, Alternating Gradient Synchrotron, AGS, to investigate particle production in p-p interactions at 28.5 GeV incident energy using a multiparticle spectrometer, MASS: Multiparticle Argo Spectrometer System.[1] Wire spark chambers and dipole magnets provide the momentum analysis of the produced particles and Cherenkov counters identify the final state protons. The spark chambers triggered by scintillation and Cherenkov counters provide selection of events and allow us to collect particle production data for event types of such small cross section, $\sim 10^{-36} cm^2$, that they have heretofore not been observed.

The analysis of $\sim 1.5 \times 10^6$ triggers has been progressing over the past year with some early results already available.[2-5] The dependence of the average charge prong multiplicity on the kinematic variables of fast recoil proton has been published.[5]

The interesting results from our early studies of the average charged multiplicity initiated this present analysis. We have extended this study by measuring the actual charged prong multiplicity distribu-

tions as a function of the kinematics variables of the fast recoil proton. The resulting corrected multiplicity data with errors, and fits to these data in parameterizations suggested by some current models are presented.

From recent bubble chamber exposures at the National Accelerator Laboratory the charge prong multiplicity distributions for proton-proton collisions at incident energies of 102[6], 205[7], 305[8], and 400[9] GeV have been reported. That those data exhibit a scaling behavior predicted by Koba, Nielsen and Olesen[10] has been one of the interesting recent particle physics results.[11] Even more recent, Barshay and Yamaguchi[12] have suggested that KNO scaling will occur not only with incident particle energy but also with the mass recoiling from a single detected final state proton. This prediction has also been verified by recent data.[13]

Here we test the KNO scaling of the charge prong multiplicity distribution as a function of both the recoil mass from, W, and the resulting transverse momentum of, $P_\perp$, (or equivalently, the four-momentum transfer to, t) the fast recoil proton.

CHAPTER II

THE EXPERIMENT AND DATA

The data analyzed here is a subset of the data taken by MASS at the BNL AGS in 1972. The MASS, shown schematically in Fig. 1, consists of three independent spectrometers each designed to momentum analyze a different type of final state particle resulting from the p-p collision. Two of the spectrometers are conventional in design having wire spark chambers before and after a bending magnet to provide momentum analysis and terminating in a Cherenkov counter to provide particle identification. A counter telescope spanning each spectrometer provides an independent trigger signal for that spectrometer. One of the spectrometers, the high momentum spectrometer, HMS, which has a small acceptance (0.33 msr) and high momentum resolution (1/4% at 28.5 GeV/c) was placed to detect a single, fast (5-28.5 GeV), forward going (0-120 mr) particle. The other spectrometer, the low momentum spectrometer, LMS, with a larger acceptance (8.46 msr) and momentum resolution (1/2% at 2.0 GeV/c) was used to measure slow (0.5-3.0 GeV) more transverse (5-90 deg) particles. The vertex spectrometer, VS, an unconventional spectrometer consisting of nine cylindrical wire chambers operating in a 10 KG field has a large acceptance (2π sr) and exceptionally high multiparticle efficiency, was used to detect and momentum analyze the produced particles.[14] A particle through one (both) of the external spectrometer(s) triggered the external spectrometer(s) as well as the VS.

By using the movable HMS arm as a trigger we were able to record events having a final state proton with four momentum transfer, t, up

to $-5.0(\text{GeV/c})^2$. Events with $|t| > 1.0\ (\text{GeV/c})^2$ are rarely seen in typical bubble chambers because of their small production cross section and that instrument's difficulty in identifying the final state proton.

The events used in the analysis presented here are taken from the single arm HMS triggers of 339 of our 780 data runs. The HMS data of an event was first analyzed to determine the momentum and origin of the fast forward proton. The origin was found by determining the point of intersection of the beam and HMS particle. Because the angle of intersection of the two tracks was characteristically small all events which appear to come from within $\pm$ 2.0 inches of the liquid hydrogen target were carried on to the second data reduction step. A cut, $W \leq 1.25$ GeV/c, was made to eliminate elastic events from the data set.

In the second step of the analysis the VS digitizings for an event were associated into tracks which were fit to circles to determine their charge and origin.[15] The final vertex for the event was defined as the point most compatable with the intersection of all detected charged tracks. Events for which this vertex did not lie within the physical dimensions of the target were rejected. Target cuts alone reduced the data set to 190K events.

Before any corrections were applied to the charged multiplicity of an individual event, all the events were binned by W and t or $P_\perp$. The bin boundaries and the number of events each contains are shown in Tables I and II. Corrections must now be made to the charge prong multiplicity determined by the track recognition program, PITRACK, because some charged particles go undetected or unrecognized. By using Monte Carlo techniques we determined that about 6% of the charged par-

ticles go undetected due to the limited solid angle of the VS.[4] Also, about 1% of the charged particles are so slow that they do not get out of the liquid hydrogen target. By visually scanning a sample of events, we determined that PITRACK is unable to recognize about 7% of the tracks which can be associated by eye.[3] These combined effects give us an expected inefficiency of about 14%, which is, on the average, about one lost prong for each six prong event.

Because we used a vertex defined by all the produced tracks to identify events from the target we had a special problem in identifying which one prong events are really from the liquid hydrogen target. In a one prong event the only particle detected was the particle which went into the HMS. There are a large number of such events for HMS particles with $P_\perp < 1.0$ GeV/c. To eliminate the one prong events which do not originate in hydrogen, the number of one prong events in each W-$P_\perp$ bin for target empty runs were compared to target full runs. With a proper normalization for beam flux this comparison yeilded the percentage of the one prongs to be accepted, as being from the target, as a function of $P_\perp$ and W.

To correct for the losses mentioned above, we use the fact that charge conservation requires each event to have a net charge of +2. The first correction is to add the minimum number of tracks to each event to bring its net charge to +2. The effect of this correction on the multiplicity distribution in three different W-$P_\perp$ bins is shown in Table III. Another correction was made to account for the loss of two charged particles of the opposite charge. The number of times two or more tracks of the same charge are missed is considered to be a mea-

sure of the number of times a pair of opposite charge tracks are missed. Thus, the second correction was applied, not to individual events, but to the distribution itself. Table III also shows the effect of this correction by indicating the final distribution which differs from the charge corrected distribution by the correction for loss of two tracks of opposite charge. The effect of these corrections on the average charge prong multiplicity, $\langle n \rangle$, is discussed elsewhere.[5] What needs to be shown here is that these corrections do not distort the charge prong multiplicity distributions in such a way that they are no longer comparable.

The effect of all the above corrections can be seen in Table IV which shows the percentage of pseudotracks for all multiplicities in each W-t and W-P_1 bin. A "pseudotrack" was a track which was added in the correction scheme. The error represents a statistical error on this number. The percent of added tracks clearly increases as the multiplicity increases. This is explained by the increased difficulty the pattern recognition code has with the more complicated events. The percent of pseudotracks for a given multiplicity does not change greatly over the whole table. To help see this we have plotted the pseudotrack correction for the 6 prong events in each data bin in Fig. 2. This is in agreement with our analysis of the track loss mentioned above. Thus, we can compare multiplicity distributions from different bins of P_1, t and W.

CHAPTER III

RESULTS AND INTERPRETATION

The doubly differential normalized charge prong multiplicity distributions, $P(n,W,t)$ and $P(n,W,P_\perp)$, presented in Table V are the only such distributions available at any energy for any interaction. In an attempt to characterize them, they are first compared to the previously measured multiplicity distributions from pp interactions over a range of energies, then they are fit to some currently popular distributions. Finally, they are compared to one another.

Figure 3 shows a comparison of the multiplicity distribution from 10^{19}, 19^{20}, 70^{21}, and 102^{6} GeV proton-proton collisions with our $P(n,W,t)$ of the same average multiplicity. The general shapes of the distributions for the same average multiplicity are much the same. It is clear that at $\langle n \rangle \underset{\sim}{>} 6$ our $P(n,W,t)$ is narrower than the 102 GeV data. As Wroblewski[16] has pointed out for pp data over a wide range of multiplicity (energy) there is a linear relation between $\langle n \rangle$ and the dispersion,

$$D \equiv (\langle n^2 \rangle - \langle n \rangle^2)^{1/2}$$

such that,

$$D = 0.585(\langle n \rangle - 1) \quad .$$

For a constant t or $P_\perp$ interval our data shows a linear relation between D and $\langle n \rangle$ for varying W.

In Fig. 4 we plot D vs. $\langle n \rangle$ in each W interval for two typical $P_\perp$ intervals: $0.0 < P_\perp < 0.5$ and $1.0 < P_\perp < 1.25$. A straight line fits the data in each $P_\perp$ interval with a confidence level > 95%.

The line $D = 0.585(\langle n \rangle - 1)$ is also drawn to show where the total pp data lie. In places where our data overlaps with this line our multiplicity distribution would look similar to the pp total multiplicity distribution. The fourth curve, not a straight line, represents the relation between D and $\langle n \rangle$ for the Possion distribution,

$$P(n) = \langle n \rangle^n \frac{e^{-\langle n \rangle}}{n!} \quad .$$

For some W and t bins the distribution would be close to Possion, but because of the non-linear relation between D and $\langle n \rangle$ for the Possion distribution there would not be a set of distributions, for a constant t or $P_\perp$ interval, which would fit the Possion distribution.

Kaiser[17] notes that the bumps in the pp total multiplicity distributions are approximately Gaussian in shape and derives a Gaussian distribution for the pairs of produced particles assuming the colliding protons behave as a large number of independent scattering centers. He then shows the pp data can be fit to a renormalized Gaussian,

$$P(n) = A \exp[a^2(n-b)^2] \quad .$$

To compare our distributions to this form for each distribution we used the 2, 4, and 6 prong events to determine a function

$$\exp(pn^2 + qn + r)$$

and then compared this function with the tails of the distribution. In some cases the actual distributions were wider and others narrower with no clear dependence on W, t, or $P_\perp$.

In trying to compare distributions, we searched for a universal function which would describe all the distributions. Of the 79 distri-

butions listed in Table V, 27 of them have five or fewer data points. To have at least one degree of freedom in most of the fits only functions with 4 or fewer parameters were considered. The function

$$P(n) = \exp[b_1 n^3 + b_2 n^2 + b_3 n + b_4]$$

represented reasonably well the data in each W-t and W-P_1 interval. The confidence level distribution is not flat enough to claim a good fit for all the data but for a wide range of W-t and W-P_1, the fit is good. In Fig. 5 the length of the line at each data bin is proportional to the confidence level of the fit.

To identify trends in the data we look at the characteristics of the curves which have been fit to the data. To the first order, the shapes of the distributions are strongly dependent on the <n> of the distribution. We plot the average charge multiplicity as a function of the maximum of $P(n,W,P_1)$ in Fig. 6 and as a function of the value of n for which $P(n,W,P_1)$ is a maximum, n_{max}, in Fig. 7. The corresponding plots for P(n,W,t) are similar to Figs. 6 and 7. In Fig. 7 we see that n_{max} is proportional to <n>. From Fig. 6 an approximate relation

$$P(n)_{max} = 2/\langle n \rangle ,$$

is in reasonable agreement with the data.

To remove <n> dependence from the P(n,W,x) distributions we "scaled" the multiplicity distributions so that

$$P'(z,W,x) = \langle n \rangle P(n,W,x)$$

where $z = n/\langle n \rangle$ and x is t or P_1. This type of scaled multiplicity distribution was introduced by Koba, Nielsen, and Olesen in connection

with the scaling, in energy, of pp multiplicity distribution.[10] While their theoretical basis for suggesting that the scaled multiplicity distributions from different energy pp interactions will fall on a universal curve is now in question, the data from 50 to 300 GeV does indeed seem to lie along the same curve.[11]

The P' distributions were fit to the same functional form which we used on the P(n,W,x) distributions

$$P'(z,W,x) = \exp[b_1 z^3 + b_2 z^2 + b_3 z + b_4] \quad .$$

We find that all the fitted functions have $P'(z,W,x)_{max} \approx 2.0$ at a $z \approx 0.95$ so there is strong indication the P' will follow the same curve.

Figure 8 is a plot of $P'(z,W,t)$ and $P'(z,W,P_1)$ where different W intervals for the same P_1 or t interval have been drawn on the same plot. The number of points in the fit and χ^2 for the plots are listed in Table VI.

Plots of this kind can be found in the current literature dealing with different types of multiplicity scaling. See for example references 11, 13, and 18. The question as to whether the data does indeed scale, i.e. fall on the same curve, is answered sometimes by presenting χ^2 for a fit to the data, sometimes by displaying the moments of the P' distributions or even by some "eyeball fit" to a representative curve.

Before making claims for or against scaling, further investigation of the data and the fits must be made to determine if the large χ^2 is due to scatter in each doubly differential distribution or is a result of trying to force points from different curves to lie on one curve.

We will also determine whether the fits improve if one range of recoil mass is excluded.

Table VI has listed the total χ^2 for fits to the doubly differential $P'(z,W,x)$ distributions, the number of points, and number of fits involved. The sum of the χ^2 is what one would obtain if all the best fits to the individual $P'(z,W,x)$ were independent of W. We see that the $P'(z,W,x)$ are not independent of W over $P_\perp$ intervals but are independent of W over t intervals, with the possible exception for $t < 1.0(GeV/c)^2$ the high recoil mass points seem to systematically lie off the curve in both plots. They follow a curve which is lower and wider. If these points are taken out of the fit, the χ^2 per degree of freedom improves dramatically as can be seen in the last two entries in Table VI. The same systematic deviation from the fitted curve of the high recoil mass points can be seen in the plot for $0.5 < P_\perp > 0.75$. Here the removal of two sets of points from high recoil mass brings the χ^2 per degree of freedom down from 6.4 to 1.85. There was no improvement in other P ranges.

From the above analysis of the fits to the $P'(z,W,x)$ distribution we claim that the $P'(z,W,P_\perp)$ are not independent of W, that is, do not scale. $P'(z,W,t)$ distributions do scale in W with some deviation for large W at small t.

We looked for a scaling in t and P by plotting $P(z,W,x)$ for fixed W bins allowing the t and $P_\perp$ to vary. Based on the same type of χ^2 analysis, we see no approximate scaling in either t or P for fixed W.

In the fits to the $P(z,W,t)$ distributions, one notices the curves getting narrower with the peak shifting toward higher z as $|t|$ increases.

The shape differences in the distributions can be seen directly by comparing two distributions with the same <n> but different W and t values, the one with the larger t we expect to be narrower. Two such pairs of distributions are plotted in Fig. 9 and the expected shape difference is evident.

The change in shape of P(n,t) as a function of t, seen in Fig. 10, shows the trend for P'(n,t) to be higher, and narrower, at large $|t|$. However, the mean W in each t bin is also increasing as $|t|$ increases so the data points are not independent of W.

There has recently been a great deal of interest in the shapes of pp→p+ANYTHING multiplicity distributions as a function of W.[13,18] For comparison with others we have plotted in Fig. 11 n/<n> vs. <n> P(n,W,t) summed over t for our six intervals of W. The fit of our polynomial exponential to these 44 data points is poor, $\chi^2 \sim 360$. Visually, the points may seem to be on a common curve but because the errors, which are statistical only, are small so that the slight scatter of the point gives the large χ^2.

In Fig. 12 we present our data in the same fashion as Barshay et al.[13] by plotting N/<N> vs. <N>P(N,W) where the N and <N> are the associated multiplicity and average associated multiplicity, that is the multiplicity of the recoil blob,

$$N = n - 1.$$

P(N,W) does not scale in W over all W, however, there might be approximate scaling in the three highest W bins. While this result is not in contradiction with the conclusion of Barshay et al., it should be pointed out that the deviation for the low recoil mass points does not occur

for the <n>P(n,W) distribution. It is clear that the shift of variables from n to N will tend to widen and lower the curves with lower <n> more than those with larger <n>.

CHAPTER IV

FUTURE DIRECTION

The dependency of the number of charged particles produced in a pp collision on the kinematic variables of one of the recoil protons is not understood. While it appears that these dependencies are best studied by looking at scaled distributions, the details of just what distributions are important are unknown. It is not clear whether the total number of charged particles produced or the number of charged particles in the blob under consideration should be used in studying the multiplicity variation. The variable of variables in which one should look for scaling are unknown because there has been little or no theoretical speculation in these areas.

As we continue to analyze more of our data and include the LMS trigger events in our data sample, we should be able to examine some of the above problems with more events and hence finer binning. This increased data resource should permit us to make firmer statements on the shapes of the charge multiplicity distributions as a function of the kinematics of the identified proton.

APPENDIX

ONLINE MONITORING OF THE EXPERIMENT

MASS, an extremely complex experimental device, required extensive and time critical monitoring for its successful operation and effective employment. A dedicated PDP-9 at the experiment site monitored a small part of the data in real time while collecting substantially more which it transmitted via a high speed data link, BROOKNET, to a remote CDC-6600 computer. There, detailed analysis of the data was performed. The results were shipped back to the experiment for display and printing with typical turn-around times of 20 minutes. Here we describe the construction of the software executed in the CDC-6600 which monitored MASS: the ONLINE code.

ONLINE was written in Fortran for ease in its modification. Its results were selectively available at the CDC-6600 or the experiment. The ONLINE output was used to evaluate the functioning of individual pieces of equipment, the performance of the entire system, and the physics quantity and quality of the data being gathered. Because ONLINE was run in near-real time the code had to be error free, fast, and produce output that was both intelligible and economical. ONLINE was also used as the first program in the offline analysis chain.

The program was written as the individual components of the MASS were built, tested, and modified so its monitoring functions changed in time as the operating characteristics of the components were discovered. Thus, the ONLINE code has evolved thru many cycles of growth and development.

The ONLINE code, written to run at the Brookhaven National Laboratory Central Scientific Computing Facility, had available in each of two CDC-6600 computers 64K 60 bit words of fast core memory, 100K words of directly addressable extended core memory, and millions of words of mass storage. The CDC-6600's run under the SCOPE operating system in a time sharing mode with up to seven jobs being processed in the central memory at a time. To execute ONLINE without high priority charges constrained its length to be limited to 32K words. By dividing it into four sequential programs which communicated thru mass storage files, this size was achieved. The overall flow diagram with field length requirements appears as Fig. 14. The times indicated are average clock time for the analysis of 2,500 events.

To make best use of BROOKNET hardware, large data blocks were shipped. The SETUP program arranged the data into blocks of a size which corresponded to those written on magnetic tape at the experiment site. Thus, the read/unpack ONLINE routines were independent of the data source.

The second program, INIT, initialized scalars, histogram vectors, and scatter plot fields; read in the control; calculated geometrical survey constants; and using the data, performed some fine adjustments of the survey constants of the spectrometers. Operating on the principle that constants will vary, all constants could be set from the data cards, but, default values were provided. Execution of ONLINE from the PDP-9 permitted data cards and the source code to be changed remotely for any run. In practice only about 20 of a possible 300 constants

were read from cards.

A precise line up of individual spectrometer components was then obtained when a portion of the data was read, unpacked, and partially analyzed. The modularized structure of the code proved extremely useful as the subprograms used here were also used in the next program. The final chore for INIT was to write on a scratch file initialized constants for later use.

In the third program, ACC, read, unpacked, and analyzed data event by event. The parameters for the control of this program are read from the scratch file written by INIT. After reading/unpacking the accumulation of statistics proceeded in four distinct phases: one for each spectrometer and one for the event tag words. The main driver program of each section called calculational subroutines, performed tests, kept counts and contained logic. It was the changing of these counts which first alerted the experimenters to equipment malfunctions. Concentrating all the logic into the four driven programs was extremely helpful to the understanding of the program flow. A number of the tested quantities were histogramed so that, if needed, their distribution could be output.

Figure 14 is the flow diagram of the main driver program for the HMS, HMSBOSS. It is typical of the four driver routines. The flow is linear with functional subprograms for calculations called directly. The functional subprogram structure facilitated changes. For example, the decision to use an elaborate Runge-Kutta scheme to track the HMS detected particle thru the magnetic field of the VS required the re-

writing of only one HMS subroutine.

The survey constants were available in labled common while the variables for each event were provided in the subprogram arguments. Further, the common in each subprogram only contained variables which it used. This practice facilitated the reading of the FORTRAN code.

After the last event was processed the initialization constants, counters, histograms, and plots were written onto a data file to be analyzed by the final program, PRINT. A second output file was written to provide a display of individual events on a memoryscope at the experiment site. This file contained VS spark coordinates and was useful in obtaining a quick estimate of how well that complex device was operating.

The PRINT routine did all the formating for the data which was printed. Because the output was used to identify hardward problems, it was structured so as to be emminently readable. Thus, the most important quantities occurred first. Different print levels for each section of ACC were available with each level containing all the information of the lower level but in more detail.

In practice, for each set of data a one page cover sheet together with a brief summary of each device was printed automatically at the experiment site. If on the basis of the information in the short output a more detailed output was needed it could be printed remotely. All the output formated for printing was printed at the central computing facility and stored for later reference. In providing useful output, a major educational effort was required to establish the meaning of the print out. A sample of the cover sheet for ONLINE and HMSBOSS

for a typical run appears in Fig. 15.

A print file, generated in the initialization stage, was produced which listed the data cards and indicated how the lineup had progressed.

The effectiveness of this monitoring scheme was proven in our 800 hour run at the AGS. Very little of the data proved to be unusable because of undetected hardware problems. The one set of data which we have yet to understand from the technical point of view was the only one taken in a configuration where we were not prepared to monitor and thus were forced to run blind.

To data, ONLINE has processed over 3 million events with still more to be done.

REFERENCES

1. J.R. Ficenec, T.S. Clifford, W.N. Schreiner, B.C. Stringfellow, W.P. Trower, E.W. Anderson, G.B. Collins, N.E. Hien, K.M. Moy, A. Ramanauskas, P. Schübelin, A. Thorndike, F. Turkot and L. von Lindern, Experimental Meson Spectroscopy, C. Baltay and A.H. Rosenfeld, eds. (Columbia University Press, 1970).

2. B.C. Stringfellow, Multiparticle Events with Identified Final State Protons Resulting From p-p Interactions at 28.5 GeV/c, (Ph.D. Thesis) Virginia Polytechnic Institute and State University, October, 1973, VPI-EEP-3-73 (unpublished).

3. W.N. Schreiner, Experimental Charge Multiplicity Distributions in Proton-Proton Interactions at 28.5 GeV/c, (Ph.D. Thesis) Virginia Polytechnic Institute and State University, October, 1973, VPI-EEP-4-73 (unpublished).

4. D.R. Gilbert, Characteristics of Particle Spectra Produced in p-p Interactions at 28.5 GeV/c, (Ph.D. Thesis) Virginia Polytechnic Institute and State University, November, 1973, VPI-EEP-6-73 (unpublished).

5. A. Ramanauskas, E.W. Anderson, G.P. Fisher, N.C. Hien, E. Lazarus, K.M. Moy, P. Schübelin, A.M. Thorndike, F. Turkot, L. von Lindern, T.S. Clifford, G.B. Collins, J.R. Ficenec, D.R. Gilbert, W.N. Schreiner, B.C. Stringfellow, W.P. Trower, A.R. Erwin, G.P. Larson, L.J. Gutay, A. Laasenen, K. Stanfield, R.B. Willmann, E. Harvey, and W. Selove, Observation of Increasing Charged Multiplicity as a Function of Transverse Momentum in 28.5 GeV/c p-p Interactions, Phys. Rev. Letters 31, 1371 (1973).

6. J.W. Chapman, N. Green, B.P. Roe, A.A. Seidl, D. Sinclair, J.C. Vander Velde, C.M. Bromberg, D. Cohen, T. Ferbel, P. Slattery, S. Stone, and B. Werner, Measurement of the Charged-Particle Multiplicity in pp Collisions at 102 GeV/c, Phys. Rev. Letters 29, 515 (1972).

8. F.T. Dao, D. Gordon, J. Lach, E. Malamud, T. Meyer, R. Poster and W. Slater, pp Interactions at 303 GeV/c: Multiplicity and Total Cross Section, Phys. Rev. Letters 29, 1627 (1972).

9. C. Bromberg, D. Chaney, D. Cohen, T. Ferbel, P. Slottery, D. Underwood, J.W. Chapman, J.W. Cooper, N. Green, B.P. Roe, A.A. Seidl and J.C. Vonder Velde, Cross Sections and Charged-Particle Multiplicities at 105 and 405 GeV/c, Phys. Rev. Letters 31, 1563 (1973).

10. Z. Koba, H.B. Nielsen, and P. Olesen, Scaling of Multiplicity Distributions in High Energy Hadron Collisions, Nucl. Phys. B40, 317 (1972).

11. P. Slattery, Evidence for the Onset of Semi-inclusive Scaling in Proton-Proton Collisions in the 50-300 GeV/c Momentum Range, Phys. Rev. Letters 29, 1624 (1972).

12. B. Barshay and Y. Yamaguchi, ITP-SUNY, Stony Brook preprint, December 1973, (to be published).

13. S. Barshay, R. Engelman, T. Kafka, M. Pratap, Y. Yamaguchi, S.J. Borish, D.C. Colley, P. Schultz, and J. Whitmore, Approximate Scaling of Multiplicity Distributions as a Function of Missing Mass, ITP-SUNY, Stony Brook preprint, April 1974, (to be published).

14. J.R. Ficenec, B.C. Stringfellow, G.B. Collins, A. Ramanauskas, P. Schübelin, and F. Turkot, Magnetic Multiparticle Spectrometer Using Digitized Cylindrical Spark Chambers, Nucl. Inst. & Methods 113, 535 (1973).

15. D.R. Gilbert, W.N. Schreiner, W.P. Trower and P. Schübelin, Track Recognition Code for a Magnetic Multiparticle Spectrometer, Nucl. Inst. & Methods 116, 501 (1974).

16. A. Wroblewski, Proceedings of the Cracow Summer School 1973, (to be published).

17. G.D. Kaiser, Multiplicity Distributions of Charged and Neutral Particles-A Brief Review, GIFT, August, 1973. (unpublished)

18. J. Whitmore and M. Derrick, Multiplicity Distributions in the Reaction p+p→p+ANYTHING, NAL-Pub-74/30 Exp. 7200.4 1, March 1974, (to be published).

19. S.P. Almeida, J.G. Rushbrooke, J.H. Scharenguivel, M. Behrens, V. Blobel, I. Borecha, H.C. Dehne, J. Diaz, G. Knics, A. Schmitt, K. Strömer, W.P. Swanson, pp Interactions at 10 GeV/c, Physical Review 174, 1638, (1968).

20. H. Boggild, E. Dahl-Jensen, K.H. Hansen, J. Johnstod, E. Lohse, M. Suk, L. Veje, U.J. Karimaki, K.V. Laurihainen, E. Riipinen, T. Jacobsen, S.O. Sorensen, J. Allon, G. Blomquest, O. Donlelsing, G. Ehspong, L. Granstorm, S.O. Holmgren, S. Nilsson, B.E. Ronne, U. Siedins, N.K. Yomdagnu, Some Features of Particle Multiplicities and Momentum Spectra in Inelastic Proton-Proton Collisions at 19 GeV/c, Nucl. Phys. B27, 285 (1971).

21. Soviet-French Collaboration, XVI Internal Conference on High Energy Physics Paper 752 (1972).

Table IA. Number of Events and Average Charge Multiplicity for W-t Intervals.

$-t(GeV^2/c^2)$	W(GeV) 1.2	2.0	3.0	4.0	5.0	6.0
0.0	4070 2.83±.03	6346 3.62±.02	7053 4.16±.02	4600 4.56±.03		
0.5	1069 2.80±.05	3097 3.62±.03	6267 4.25±.03	8159 4.77±.02	3442 5.10±.04	
1.0	1091 2.83±.05	2723 3.59±.04	7864 4.32±.02	20426 4.99±.02	8758 5.45±.02	
1.5	365 2.94±.09	1438 3.57±.05	5620 4.34±.03	21659 5.04±.02	12226 5.53±.02	95 5.77±.25
2.0	100 2.70±.16	447 3.71±.09	2099 4.51±.05	8029 5.16±.03	7423 5.77±.03	258 6.23±.16
2.5	34 3.00±.30	172 3.63±.15	796 4.65±.08	1618 5.37±.06	4965 6.04±.03	435 6.17±.12
3.0	12 3.00±.50	66 4.03±.25	214 4.86±.15	1032 5.70±.07	4928 6.23±.04	1391 6.38±.07
3.5		13 4.77±.61	193 4.79±.16	2175 5.70±.05	14965 6.43±.02	1140 6.37±.07
4.0						

Table IB. Average W(GeV) and Average $t(GeV^2/c^2)$ for W-t Intervals.

$-t(GeV^2/c^2)$	W(GeV) 1.2	2.0	3.0	4.0	5.0	6.0
0.0						
	1.66	2.53	3.50	4.38		
	.24	.22	.27	.38		
0.5						
	1.67	2.58	3.55	4.50	5.23	
	.78	.82	.83	.77	.80	
1.0						
	1.68	2.57	3.60	4.55	5.24	
	1.19	1.21	1.22	1.24	1.34	
1.5						
	1.69	2.59	3.62	4.59	5.25	6.05
	1.70	1.71	1.70	1.73	1.72	1.89
2.0						
	1.72	2.59	3.62	4.55	5.42	6.10
	2.20	2.19	2.21	2.19	2.22	2.27
2.5						
	1.75	2.61	3.62	4.51	5.63	6.08
	2.72	2.72	2.70	2.68	2.74	2.82
3.0						
	1.65	2.59	3.58	4.70	5.53	6.09
	3.18	3.20	3.19	3.32	3.30	3.27
3.5						
		2.63	3.66	4.69	5.58	6.14
		3.68	3.77	3.74	3.77	3.69
4.0						

Table IIA. Number of Events and Average Charge Multiplicity for W-$P_\perp$ Intervals.

$P_\perp$(GeV/c)	W(GeV) 1.2	2.0	3.0	4.0	5.0	6.0
0.00	2650 2.89±.03	4802 3.68±.03	6025 4.17±.03	6759 4.70±.03	4324 5.30±.04	453 6.03±.12
0.50	1603 2.71±.04	2005 3.47±.04	3078 4.23±.04	13218 4.95±.02	1799 5.67±.02	9674 6.70±.03
0.75	1097 2.82±.05	3880 3.63±.03	10965 4.30±.02	32899 5.03±.01	32306 6.14±.01	5575 6.80±.03
1.00	1062 2.84±.05	2623 3.57±.04	7949 4.35±.02	11880 5.06±.02	17299 6.33±.02	
1.25	272 2.89±.10	832 3.62±.07	1811 4.59±.05	4558 5.73±.04	2126 6.20±.05	
1.50	48 2.92±.25	157 3.82±.16	491 4.84±.10	1036 5.71±.07		
1.75		41 4.54±.33	161 4.93±.18	31 4.77±.39		
2.00		16 4.50±.53				
2.25						

Table IIB. Average W(GeV) and Average $P_\perp$(GeV/c) for W-$P_\perp$ Intervals.

$P_\perp$(GeV/c)	W(GeV) 1.2	2.0	3.0	4.0	5.0	6.0
0.00	1.67	2.54	3.51	4.51	5.37	6.13
	.40	.37	.37	.39	.40	.40
0.50	1.65	2.51	3.58	4.61	5.40	6.20
	.59	.60	.63	.67	.67	.66
0.75	1.67	2.58	3.59	4.58	5.57	6.08
	.90	.89	.87	.88	.87	.80
1.00	1.68	2.57	3.59	4.43	5.43	
	1.10	1.12	1.10	1.09	1.10	
1.25	1.69	2.55	3.55	4.67	5.15	
	1.34	1.34	1.34	1.36	1.31	
1.50	1.71	2.55	3.63	4.40		
	1.60	1.58	1.62	1.58		
1.75		2.66	3.56	4.12		
		1.87	1.84	1.78		
2.00		2.63				
		2.10				
2.25						

Table IIIA. Uncorrected, Charge Corrected, and Final Charge Prong Multiplicities for $2.0 < W \leq 3.0$ GeV and $0.50 < P_{\perp} \leq 0.75$ GeV/c.

Charge Uncorrected	Σ→	Charge Corrected 2	4	6	8	10
1	728	728	-	-	-	-
2	668	593	75	-	-	-
3	371	-	364	7	-	-
4	535	-	485	50	-	-
5	85	-	-	82	3	-
6	50	-	-	46	4	-
7	3	-	-	-	3	-
8	2	-	-	-	1	1
Σ↑		1321	924	185	11	1
Final		1246	942	235	17	2

Table IIIB. Uncorrected, Charge Corrected, and Final Charge Prong Multiplicities for $3.0 < W \leq 4.0$ GeV and $1.25 < P_\perp \leq 1.50$ GeV/c.

Charge Uncorrected	Σ→	Charge Corrected 2	4	6	8	10	12	14
1	505	505	-	-	-	-	-	-
2	1653	1417	236	-	-	-	-	-
3	1542	-	1514	38	-	-	-	-
4	2302	-	2147	255	-	-	-	-
5	961	-	-	920	41	-	-	-
6	660	-	-	556	97	7	-	-
7	136	-	-	-	119	16	1	-
8	52	-	-	-	29	17	5	1
9	16	-	-	-	-	12	2	2
10	1	-	-	-	-	-	1	-
11	1	-	-	-	-	-	1	-
Σ↑		1922	3897	1769	292	56	10	3
Final		1686	3840	1918	392	91	16	6

Table IIIC. Uncorrected, Charge Corrected, and Final Charge Prong Multiplicities for $4.0 < W \leq 5.0$ GeV and $1.25 < P_\perp \leq 1.50$ GeV/c.

Charge Uncorrected	Σ→	Charge Corrected 2	4	6	8	10	12	14	16
1	88	88	-	-	-	-	-	-	-
2	376	315	61	-	-	-	-	-	-
3	532	-	493	39	-	-	-	-	-
4	1248	-	1011	232	5	-	-	-	-
5	848	-	-	185	61	2	-	-	-
6	882	-	-	675	198	8	1	-	-
7	354	-	-	-	316	35	3	-	-
8	173	-	-	-	120	42	11	-	-
9	39	-	-	-	-	36	3	-	-
10	14	-	-	-	-	7	6	1	-
11	0	-	-	-	-	-	-	-	-
12	3	-	-	-	-	-	1	2	-
13	0	-	-	-	-	-	-	-	-
14	1	-	-	-	-	-	-	-	-
Σ↑		403	1565	1731	700	130	25	3	1
Final		342	1355	1738	877	193	46	5	2

Table IVA. Percent of Pseudotracks for 2,4,6,8,10,12, 14, and 16 Prong Events in Each W-t Bin.

$-t(GeV^2/c^2)$	W(GeV) 1.2	2.0	3.0	4.0	5.0	6.0
0.0	6.5± 0.4	12.9± 0.5	26.3± 0.9	32.1± 1.2	0	0
	24.1± 0.7	18.2± 0.4	18.9± 0.4	21.6± 0.6	0	0
	30.9± 2.1	23.0± 0.7	20.1± 0.5	20.6± 0.5	0	0
	31.9± 4.7	25.0± 2.1	22.3± 1.0	22,0± 0.8	0	0
	27.1± 6.2	44.3± 8.0	25.2± 2.9	26,0± 1.9	0	0
	0	23.5± 4.2	30.6± 6.5	29,1± 4.9	0	0
	0	0	0	28,6± 5.8	0	0
	0	0	0	0	0	0
0.5	9.3± 0.8	12.0± 0.7	17.0± 0.8	25.4± 0.9	32.4± 1.6	0
	21.5± 1.3	15.1± 0.5	15.7± 0.4	20.6± 0.4	23.6± 0.7	0
	32.8± 4.1	20.8± 0.9	17.3± 0.5	19.3± 0.4	20.6± 0.6	0
	31.3± 7.0	28.0± 3.1	22.4± 1.0	21.7± 0.6	21.8± 0.7	0
	0	22.2± 3.5	25.1± 2.0	24.8± 1.3	24.5± 1.6	0
	0	0	31.8± 4.1	25.4± 3.0	25.0± 3.6	0
	0	35.7±11.3	42.9±12.4	35.7±11.3	21.4± 8.8	0
	0	0	0	0	0	0
1.0	8.8± 0.8	11.1± 0.8	14.0± 0.6	15.8± 0.5	16.6± 0.9	0
	20.6± 1.2	14.7± 0.5	15.0± 0.3	17.7± 0.2	20.1± 0.4	0
	26.8± 3.7	19.6± 1.0	17.4± 0.4	18.7± 0.2	19.9± 0.3	0
	25.0±10.2	29.0± 2.6	22.5± 0.9	21.5± 0.3	20.9± 0.4	0
	30.0±17.3	24.0± 4.9	26.9± 1.7	23.2± 0.7	23.8± 0.8	0
	25.0±10.2	0	25.6± 4.1	26.9± 1.6	29.7± 1.9	0
	0	0	28.6±10.1	30.6± 4.0	25.0± 3.0	0
	0	0	0	0	0	0
1.5	8.8± 1.4	11.5± 1.1	15.1± 0.8	16.8± 0.5	16.9± 0.8	16.7± 8.9
	17.8± 1.8	13.7± 0.7	15.9± 0.4	18.8± 0.2	19.5± 0.4	22.4± 4.4
	26.2± 7.9	21.6± 1.5	18.4± 0.5	21.3± 0.2	20.8± 0.3	24.3± 4.1
	0	25.0± 4.2	24.4± 1.1	22.8± 0.3	22.5± 0.4	24.5± 3.5
	43.3±12.0	10.0± 0.0	28.3± 2.0	26.9± 0.8	23.5± 0.7	21.4± 5.5
	25.0±10.2	25.0±10.2	29.5± 4.4	30.3± 1.5	28.2± 1.5	0
	0	0	38.1± 6.7	31.1± 3.6	27.9± 3.1	0
	0	0	0	37.5±10.8	37.5±10.8	0
2.0	3.8± 1.7	13.1± 2.1	12.2± 1.3	14.9± 0.9	17.3± 1.2	14.5± 7.1
	12.9± 3.1	14.2± 1.3	14.8± 0.6	18.5± 0.4	21.3± 0.5	22.3± 2.9
	16.7±16.7	21.5± 2.4	18.6± 0.7	20.6± 0.3	22.4± 0.4	21.4± 2.0
	0	28.1± 6.6	24.4± 1.5	23.4± 0.5	23.1± 0.5	23.3± 2.3
	0	40.0±14.1	23.7± 3.5	25.7± 1.3	24.7± 0.8	23.2± 2.7
	0	0	0	31.3± 2.7	26.3± 2.0	41.7±13.2
	0	0	0	28.6± 5.0	32.7± 4.1	0
	0	0	0	0	0	0
2.5	2.8± 2.8	7.4± 2.5	9.5± 1.9	12.6± 1.9	15.6± 1.5	10.8± 3.8
	11.7± 4.4	12.4± 2.0	14.1± 1.0	16.8± 0.9	20.7± 0.6	25.0± 2.7
	16.7±16.7	19.4± 3.7	21.0± 1.2	21.2± 0.8	22.0± 0.5	22.5± 1.5
	0	12.5±12.5	25.2± 2.4	22.8± 1.1	24.8± 0.5	23.4± 1.6
	0	0	38.9± 6.6	24.2± 2.2	24.4± 0.8	24.5± 2.5
	0	0	41.7±13.2	26.7± 4.7	25.0± 1.9	16.7± 5.9
	0	0	0	0	35.7± 5.1	0
	0	0	0	0	31.3± 7.0	0
3.0	25.0±14.4	12.5± 5.6	7.4± 3.3	7.9± 2.3	18.7± 2.0	15.7± 3.1
	20.8± 9.3	17.2± 3.9	12.8± 2.0	14.4± 1.1	18.9± 0.6	23.1± 1.4
	0	24.4± 5.6	21.4± 2.3	20.4± 0.9	22.0± 0.5	22.0± 0.9
	0	37.5±10.8	22.8± 3.2	21.2± 1.1	23.3± 0.5	24.2± 0.9
	0	0	10.0±10.0	25.1± 2.7	24.8± 0.8	25.4± 1.5
	0	0	0	12.5± 7.2	26.4± 1.7	28.3± 2.9
	0	0	0	25.0± 6.7	25.5± 3.6	21.4± 5.5
	0	0	0	0	43.8±11.7	18.8± 7.6
3.5	0	0	7.1± 3.6	13.3± 2.0	16.0± 1.1	16.7± 3.9
	0	22.2± 7.9	12.5± 1.9	12.7± 0.7	15.9± 0.4	21.9± 1.5
	0	27.8±12.4	16.4± 2.1	16.8± 0.6	19.4± 0.2	24.2± 1.0
	0	12.5±12.5	20.8± 4.2	20.4± 0.8	21.3± 0.3	24.5± 1.0
	0	0	30.0± 8.7	22.0± 1.5	23.8± 0.4	27.4± 1.9
	0	0	0	26.7± 3.3	27.2± 0.8	25.3± 2.9
	0	0	0	28.6±14.3	30.5± 1.9	23.2± 4.6
	0	0	0	12.5± 6.3	32.8± 5.1	0
4.0						

Table IVB. Percent of Pseudotracks for 2,4,6,8,10,12, 14, and 16 Prong Events in Each W-P_t Bin.

P_t(GeV/c)	W(GeV) 1.2	2.0	3.0	4.0	5.0	6.0
0.00	3.4± 0.3	10.4± 0.6	25.8± 0.9	31.6± 1.1	31.2± 1.5	15.4± 4.4
	24.1± 0.8	18.5± 0.4	18.9± 0.4	22.3± 0.5	23.1± 0.7	22.3± 2.3
	30.1± 2.5	23.0± 0.8	19.7± 0.5	20.5± 0.4	20.8± 0.5	24.1± 1.6
	30.4± 5.2	24.6± 2.3	22.5± 1.1	22.0± 0.7	22.2± 0.6	23.4± 1.6
	30.0± 7.1	44.3± 8.0	25.0± 3.1	25.1± 1.4	23.6± 1.2	22.7± 2.5
	0	23.5± 4.2	30.6± 6.5	27.3± 3.6	25.4± 3.3	29.2± 7.8
	0	0	0	28.6± 5.8	16.7± 4.5	0
	0	0	0	0	0	0
0.50	11.5± 0.7	18.0± 1.1	23.9± 1.3	19.8± 0.7	15.8± 0.6	17.4± 1.4
	23.8± 1.1	17.4± 0.7	17.5± 0.6	18.9± 0.3	20.4± 0.3	21.3± 0.6
	30.4± 3.6	22.8± 1.3	19.5± 0.7	18.9± 0.3	20.4± 0.2	22.0± 0.3
	37.5±10.8	27.2± 4.5	21.3± 1.3	21.6± 0.4	22.3± 0.3	23.4± 0.3
	10.0±10.0	20.0±10.0	24.2± 3.2	23.9± 0.8	23.5± 0.5	24.7± 0.5
	0	0	28.3± 6.9	26.5± 2.1	28.0± 1.1	26.2± 0.9
	0	0	0	31.4± 4.7	28.6± 2.1	26.3± 1.9
	0	0	0	0	37.5±10.8	32.8± 3.6
0.75	9.0± 0.8	11.2± 0.6	14.4± 0.5	16.5± 0.4	17.6± 0.6	16.0± 1.9
	21.3± 1.2	14.7± 0.4	14.9± 0.3	18.5± 0.2	19.2± 0.2	18.6± 0.7
	34.3± 4.0	20.1± 0.9	17.2± 0.3	20.3± 0.2	20.8± 0.2	20.8± 0.4
	31.3± 7.0	28.7± 2.5	22.4± 0.7	22.4± 0.3	22.3± 0.2	21.5± 0.4
	10.0± 0.0	23.6± 3.3	26.4± 1.4	25.1± 0.6	24.0± 0.3	23.4± 0.6
	25.0±10.2	0	29.0± 3.4	28.9± 1.2	27.2± 0.7	26.7± 1.1
	0	35.7±11.3	35.7± 8.0	32.3± 3.2	30.3± 1.6	27.8± 2.6
	0	0	0	37.5±10.8	30.2± 4.0	34.4± 5.2
1.00	8.8± 0.8	11.6± 0.8	15.0± 0.7	15.5± 0.7	16.5± 1.0	0
	19.7± 1.2	14.2± 0.5	15.8± 0.3	17.6± 0.3	15.3± 0.3	0
	26.3± 4.1	20.8± 1.1	18.4± 0.4	20.6± 0.3	19.2± 0.2	0
	34.4±10.4	26.4± 2.7	24.2± 0.9	22.9± 0.5	21.4± 0.3	0
	25.0± 7.9	23.3± 8.8	28.2± 1.8	26.2± 1.1	23.6± 0.4	0
	0	25.0±10.2	29.7± 3.9	32.5± 2.6	27.3± 0.8	0
	0	0	38.1± 6.7	25.0± 3.9	29.5± 2.0	0
	0	0	0	0	40.6± 5.6	0
1.25	8.5± 1.6	12.1± 1.4	9.8± 1.2	12.9± 1.4	12.0± 2.4	0
	17.3± 2.1	14.1± 0.9	14.2± 0.7	12.9± 0.5	14.1± 0.8	0
	23.3± 8.8	21.8± 1.9	20.4± 0.8	18.0± 0.4	18.3± 0.6	0
	25.0± 7.7	29.2± 4.9	25.4± 1.6	20.8± 0.5	21.1± 0.7	0
	70.0±26.5	40.0±14.1	28.8± 4.1	23.8± 1.1	22.6± 1.2	0
	25.0±10.2	0	41.7±13.2	30.8± 2.4	29.0± 3.1	0
	0	0	0	22.9± 5.7	35.7±11.3	0
	0	0	0	12.5± 6.3	0	0
1.50	7.4± 3.7	9.0± 3.0	12.1± 3.0	9.5± 2.8	0	0
	15.0± 4.3	13.3± 2.1	12.2± 1.2	13.6± 1.0	0	0
	16.7±16.7	21.3± 3.8	17.0± 1.4	17.7± 0.9	0	0
	0	37.5±10.8	21.4± 2.5	20.3± 1.2	0	0
	0	0	30.0± 4.8	25.1± 2.5	0	0
	0	0	0	30.6± 5.3	0	0
	0	0	0	35.7±11.3	0	0
	0	0	0	0	0	0
1.75	0	10.0±10.0	7.1± 5.1	0	0	0
	0	13.1± 4.0	10.2± 1.9	8.3± 3.7	0	0
	0	22.6± 5.2	17.2± 2.1	22.9± 6.9	0	0
	0	12.5±12.5	20.2± 4.4	15.6± 7.0	0	0
	0	0	0	0	0	0
	0	0	0	0	0	0
	0	0	0	0	0	0
	0	0	0	0	0	0
2.00	0	0	0	0	0	0
	0	9.4± 5.4	0	0	0	0
	0	5.6± 5.6	0	0	0	0
	0	25.0±12.5	0	0	0	0
	0	0	0	0	0	0
	0	0	0	0	0	0
	0	0	0	0	0	0
	0	0	0	0	0	0
2.25						

Table VA. Final Charge Prong Multiplicity Distribution, P(n), in Percent, for 2,4,6,8,10,12,14, and 16 Prong Events in Each W-t Bin.

-t(GeV^2/c^2)	W(GeV) 1.2	2.0	3.0	4.0	5.0	6.0
0.0	62.9± 1.8	34.7± 1.2	25.1± 1.1	23.8± 1.3	0	0
	33.6± 0.9	51.7± 0.9	46.8± 0.9	37.7± 1.0	0	0
	2.9± 0.3	12.2± 0.5	23.4± 0.6	27.7± 0.8	0	0
	0.4± 0.1	1.2± 0.1	4.1± 0.3	9.0± 0.5	0	0
	0.2± 0.1	0.1± 0.1	0.4± 0.1	1.5± 0.2	0	0
	0	0.2± 0.1	0.1± 0.1	0.2± 0.1	0	0
	0	0	0	0.1± 0.1	0	0
	0	0	0	0	0	0
0.5	64.4± 2.9	35.8± 1.3	24.1± 0.8	18.3± 0.7	18.5± 1.2	0
	31.9± 1.8	49.8± 1.3	47.0± 0.9	39.9± 0.7	31.4± 1.0	0
	3.0± 0.6	12.6± 0.7	22.7± 0.6	29.6± 0.6	31.0± 1.0	0
	0.8± 0.3	1.2± 0.2	5.0± 0.3	10.0± 0.4	15.8± 0.7	0
	0	0.6± 0.1	1.0± 0.1	1.9± 0.2	2.9± 0.3	0
	0	0	0.3± 0.1	0.3± 0.1	0.5± 0.1	0
	0	0.1± 0.1	0	0	0.1± 0.1	0
	0	0	0	0	0	0
1.0	63.2± 2.5	36.8± 1.3	22.5± 0.6	15.0± 0.3	12.2± 0.5	0
	33.3± 1.8	49.8± 1.4	46.8± 0.8	38.5± 0.5	31.5± 0.7	0
	3.0± 0.5	11.0± 0.7	24.4± 0.6	32.1± 0.4	34.5± 0.7	0
	0.3± 0.2	2.1± 0.3	4.9± 0.3	11.3± 0.3	16.2± 0.5	0
	0.1± 0.1	0.4± 0.1	1.2± 0.1	2.6± 0.1	4.6± 0.2	0
	0.2± 0.1	0	0.2± 0.1	0.4± 0.1	0.8± 0.1	0
	0	0	0	0.1± 0.1	0.2± 0.1	0
	0	0	0	0	0	0
1.5	59.5± 4.1	36.2± 1.6	21.6± 0.7	13.8± 0.3	10.9± 0.4	11.0± 4.8
	37.3± 3.2	50.6± 1.9	48.2± 1.0	38.4± 0.5	31.0± 0.6	30.4± 6.1
	1.9± 0.8	11.8± 0.9	23.9± 0.7	33.4± 0.4	35.4± 0.6	25.1± 6.1
	0.0± 0.4	1.3± 0.3	4.7± 0.3	11.8± 0.2	17.3± 0.4	26.2± 5.4
	0.8± 0.6	0	1.3± 0.2	2.1± 0.1	4.3± 0.2	7.3± 2.8
	0.5± 0.4	0.1± 0.1	0.2± 0.1	0.5± 0.1	0.9± 0.1	0
	0	0	0.1± 0.1	0.1± 0.1	0.2± 0.1	0
	0	0	0	0	0	0
2.0	66.0± 8.3	33.3± 2.8	18.5± 1.0	11.8± 0.4	8.4± 0.4	5.7± 2.1
	33.0± 5.7	50.6± 3.5	45.7± 1.5	37.0± 0.7	28.2± 0.7	25.1± 3.5
	1.0± 1.0	13.9± 1.8	28.1± 1.2	35.9± 0.7	37.3± 0.8	34.4± 4.0
	0	1.8± 0.7	6.7± 0.6	12.9± 0.4	19.6± 0.5	22.0± 3.2
	0	0.5± 0.3	0.9± 0.2	1.9± 0.2	5.5± 0.3	12.0± 2.2
	0	0	0	0.5± 0.1	0.8± 0.1	0.8± 0.5
	0	0	0	0.1± 0.1	0.2± 0.1	0
	0	0	0	0	0	0
2.5	52.9±12.8	35.5± 4.6	17.2± 1.5	10.3± 0.9	7.2± 0.5	8.7± 1.8
	44.1±11.4	49.4± 5.5	43.1± 2.5	34.1± 1.6	25.4± 0.8	19.3± 2.5
	2.9± 2.9	14.0± 2.9	31.2± 2.1	36.7± 1.6	36.1± 1.0	37.6± 3.3
	0	0.6± 0.6	7.2± 1.0	15.0± 1.0	22.8± 0.7	24.8± 2.6
	0	0.6± 0.6	1.1± 0.4	3.2± 0.5	7.2± 0.4	8.7± 1.5
	0	0	0.3± 0.2	0.6± 0.2	1.2± 0.2	0.9± 0.5
	0	0	0	0	0.2± 0.1	0
	0	0	0	0	0.1± 0.	0
3.0	50.0±22.1	30.3± 7.1	15.9± 2.8	7.4± 0.9	4.9± 0.4	5.8± 0.9
	50.0±20.4	43.9± 8.6	39.3± 4.6	27.8± 1.9	24.5± 0.8	20.8± 1.4
	0	19.7± 5.9	31.3± 4.1	41.4± 2.1	36.2± 1.0	36.4± 1.8
	0	6.1± 3.0	13.1± 2.5	19.9± 1.4	25.2± 0.8	25.9± 1.5
	0	0	0.5± 0.5	3.4± 0.6	7.3± 0.4	8.6± 0.8
	0	0	0	0	1.6± 0.2	2.0± 0.4
	0	0	0	0.4± 0.2	0.3± 0.1	0.4± 0.2
	0	0	0	0	0	0.1± 0.1
3.5	0	0.0± 7.7	14.5± 2.9	7.6± 0.6	4.6± 0.2	4.8± 0.9
	0	69.2±24.3	43.5± 5.1	30.9± 1.3	21.6± 0.4	21.7± 1.6
	0	23.1±13.3	32.1± 4.2	37.4± 1.4	36.3± 0.6	36.5± 2.0
	0	7.7± 7.7	7.8± 2.1	18.5± 1.0	26.1± 0.5	27.6± 1.7
	0	0	2.1± 1.0	4.5± 0.5	8.7± 0.3	6.4± 0.8
	0	0	0	0.9± 0.2	2.3± 0.1	2.3± 0.5
	0	0	0	0.1± 0.1	0.4± 0.1	0.7± 0.3
	0	0	0	0.1± 0.1	0.1± 0.1	0
4.0						

Table VB. Final Charge Prong Multiplicity Distribution, P(n), in Percent, for 2,4,6,8,10,12,14, and 16 Prong Events in Each W-P Bin.

$P_\perp$(GeV/c)	W(GeV) 1.2	2.0	3.0	4.0	5.0	6.0
0.00	60.3± 2.3	32.5± 1.5	24.6± 1.2	21.0± 1.0	16.0± 1.0	8.9± 1.9
	35.8± 1.2	53.3± 1.1	47.5± 0.9	37.7± 0.8	30.1± 0.9	24.3± 2.7
	3.1± 0.4	12.6± 0.5	23.2± 0.6	29.4± 0.7	32.2± 0.9	33.3± 3.0
	0.5± 0.2	1.3± 0.2	4.2± 0.3	9.8± 0.4	17.1± 0.7	24.5± 2.5
	0.2± 0.1	0.2± 0.1	0.4± 0.1	1.8± 0.2	4.0± 0.3	8.2± 1.4
	0	0.2± 0.1	0.1± 0.1	0.3± 0.1	0.5± 0.1	0.9± 0.4
	0	0	0	0.1± 0.1	0.1± 0.1	0
	0	0	0	0	0	0
0.50	67.5± 2.7	40.4± 2.0	25.1± 1.3	15.9± 0.5	10.6± 0.3	4.7± 0.3
	29.7± 1.4	47.0± 1.6	45.5± 1.3	38.4± 0.6	29.2± 0.5	18.2± 0.5
	2.5± 0.4	11.7± 0.8	23.4± 0.9	31.6± 0.5	35.0± 0.5	34.0± 0.7
	0.3± 0.1	0.9± 0.2	5.1± 0.4	11.1± 0.3	18.5± 0.3	28.0± 0.6
	0.1± 0.1	0.1± 0.1	0.8± 0.2	2.6± 0.2	5.3± 0.2	11.8± 0.4
	0	0	0.2± 0.1	0.4± 0.1	1.2± 0.1	2.6± 0.2
	0	0	0	0.1± 0.1	0.3± 0.1	0.6± 0.1
	0	0	0	0	0	0.2± 0.1
0.75	64.3± 2.8	35.3± 1.1	23.3± 0.6	14.2± 0.3	6.6± 0.2	4.0± 0.3
	31.6± 1.7	50.8± 1.2	46.2± 0.7	38.4± 0.4	24.7± 0.3	17.0± 0.7
	3.3± 0.6	11.8± 0.6	24.2± 0.5	32.8± 0.3	35.8± 0.4	34.9± 0.9
	0.7± 0.3	1.5± 0.2	4.9± 0.2	11.9± 0.2	23.1± 0.3	27.8± 0.8
	0	0.6± 0.1	1.2± 0.1	2.2± 0.1	7.7± 0.2	12.4± 0.5
	0.2± 0.1	0	0.2± 0.1	0.5± 0.1	1.7± 0.1	3.2± 0.3
	0	0.1± 0.1	0	0.1± 0.1	0.3± 0.1	0.5± 0.1
	0	0	0	0	0	0.1± 0.1
1.00	62.4± 2.5	37.2± 1.2	21.2± 0.6	13.3± 0.4	5.0± 0.2	0
	34.4± 1.8	49.1± 1.4	48.3± 0.8	37.7± 0.6	22.8± 0.4	0
	2.5± 0.5	11.8± 0.7	24.1± 0.6	34.9± 0.6	36.4± 0.5	0
	0.4± 0.2	1.7± 0.3	4.9± 0.3	11.7± 0.3	25.2± 0.4	0
	0.4± 0.2	0.1± 0.1	1.1± 0.1	1.9± 0.1	8.4± 0.2	0
	0	0.1± 0.1	0.2± 0.1	0.4± 0.1	1.9± 0.1	0
	0	0	0.1± 0.1	0.1± 0.1	0.3± 0.1	0
	0	0	0	0	0.1± 0.1	0
1.25	60.7± 4.8	35.8± 2.1	17.7± 1.0	7.5± 0.4	4.9± 0.5	0
	36.8± 3.7	49.6± 2.5	44.5± 1.7	29.7± 0.9	24.2± 1.2	0
	1.8± 0.8	12.5± 1.3	29.5± 1.3	38.1± 1.0	37.5± 1.5	0
	0	1.8± 0.5	7.2± 0.7	19.2± 0.7	24.0± 1.1	0
	0.4± 0.5	0.2± 0.2	0.9± 0.2	4.2± 0.3	8.1± 0.6	0
	0.7± 0.5	0	0.1± 0.1	1.0± 0.2	1.2± 0.2	0
	0	0	0	0.1± 0.1	0.1± 0.1	0
	0	0	0	0	0	0
1.50	56.3±11.2	31.9± 4.6	13.4± 1.8	6.1± 0.9	0	0
	41.7± 9.3	49.0± 5.8	45.0± 3.2	31.7± 1.9	0	0
	2.1± 2.1	15.9± 3.3	30.4± 2.6	39.3± 2.1	0	0
	0	2.6± 1.3	8.6± 1.4	18.0± 1.4	0	0
	0	0.6± 0.6	2.7± 0.7	4.0± 0.7	0	0
	0	0	0	0.9± 0.3	0	0
	0	0	0	0.2± 0.1	0	0
	0	0	0	0	0	0
1.75	0	12.2± 6.0	8.7± 2.5	12.9± 6.5	0	0
	0	51.2±12.2	44.1± 5.5	48.4±12.9	0	0
	0	34.2± 9.1	39.1± 5.1	25.8± 9.7	0	0
	0	2.4± 2.4	8.1± 2.2	12.9± 6.5	0	0
	0	0	0	0	0	0
	0	0	0	0	0	0
	0	0	0	0	0	0
	0	0	0	0	0	0
2.00	0	18.8±10.8	0	0	0	0
	0	50.0±17.7	0	0	0	0
	0	18.8±12.5	0	0	0	0
	0	12.5± 8.8	0	0	0	0
	0	0	0	0	0	0
	0	0	0	0	0	0
	0	0	0	0	0	0
	0	0	0	0	0	0
2.25						

Table VI. Summary of Fits to Scaled Multiplicity Distributions.

Interval	Number of Data Points	Overall χ^2	Percent Error Sum on b_2	Sum of χ^2	Number of Data Points	Number of Fits
$0.0 < \|t\| < 0.5$	24	71.9	9.1	10.9	24	4
$0.5 < \|t\| < 1.0$	31	65.3	10.3	16.8	27	4
$1.0 < \|t\| < 1.5$	32	36.4	5.7	18.6	32	5
$1.5 < \|t\| < 2.0$	38	57.1	6.4	28.6	38	6
$2.0 < \|t\| < 2.5$	33	33.6	9.7	20.3	30	5
$2.5 < \|t\| < 3.0$	34	16.3	13.1	6.5	31	5
$3.0 < \|t\| < 3.5$	33	23.2	10.4	11.2	27	4
$3.5 < \|t\| < 4.0$	31	23.1	7.4	16.6	28	4
$0.00 < P_\perp < 0.50$	37	100.6	12.1	14.0	37	6
$0.50 < P_\perp < 0.75$	39	224.1	7.1	22.7	39	6
$0.75 < P_\perp < 1.00$	42	316.6	5.7	33.8	42	6
$1.00 < P_\perp < 1.25$	33	183.3	6.3	19.2	31	5
$1.25 < P_\perp < 1,50$	31	46.3	5.9	6.0	31	5
$1.50 < P_\perp < 1.75$	20	7.9	11.2	0.2	17	3
$1.75 < P_\perp < 2.00$	12	1.8	31.2	--	--	--
$0.0 < \|t\| < 0.5$	17	24.9	7.7	6.2	16	3
$0.5 < \|t\| < 1.0$	24	30.2	8.6	12.1	20	3

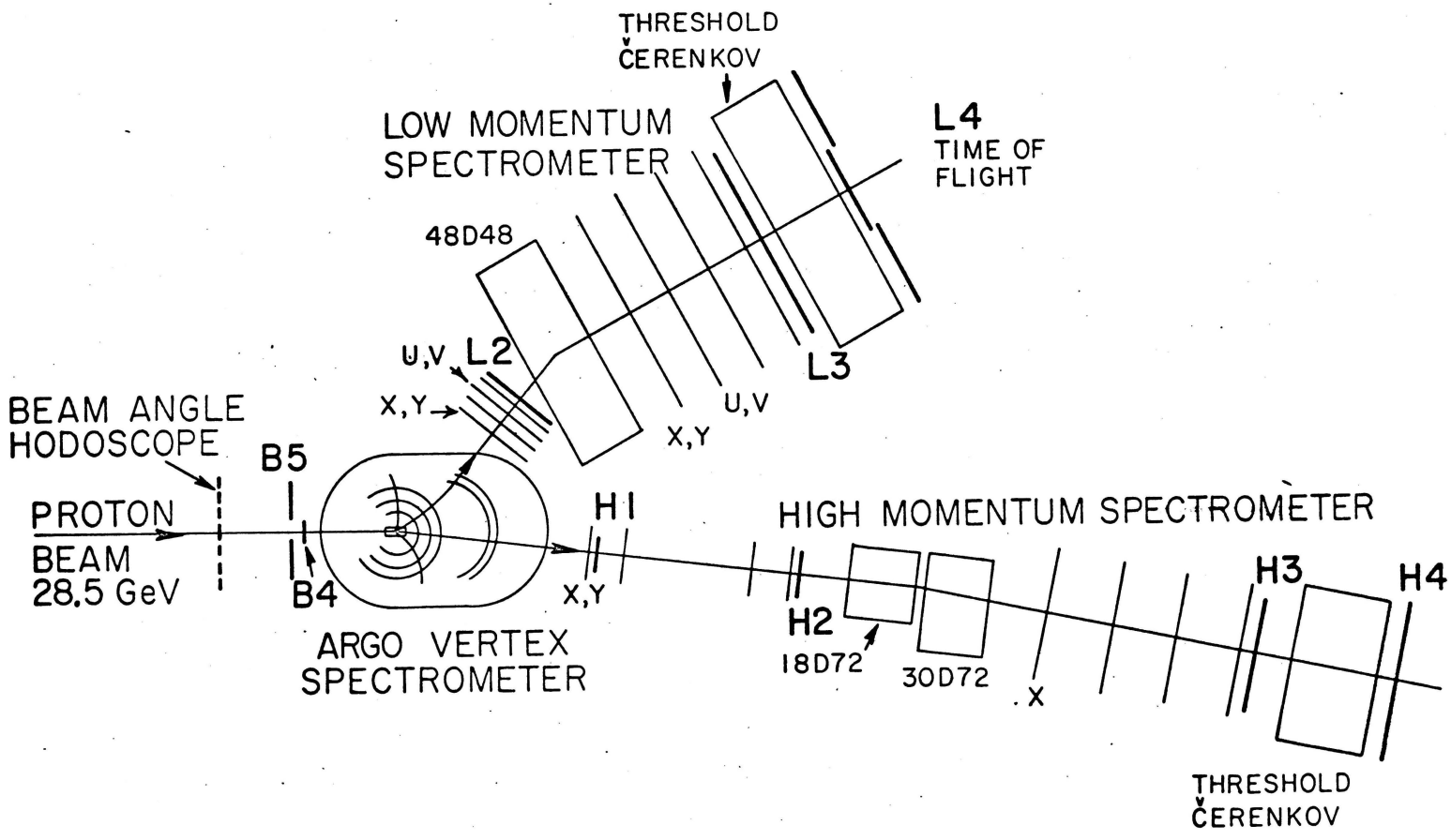

Figure 1. Schematic of the Multiparticle Argo Spectrometer System.

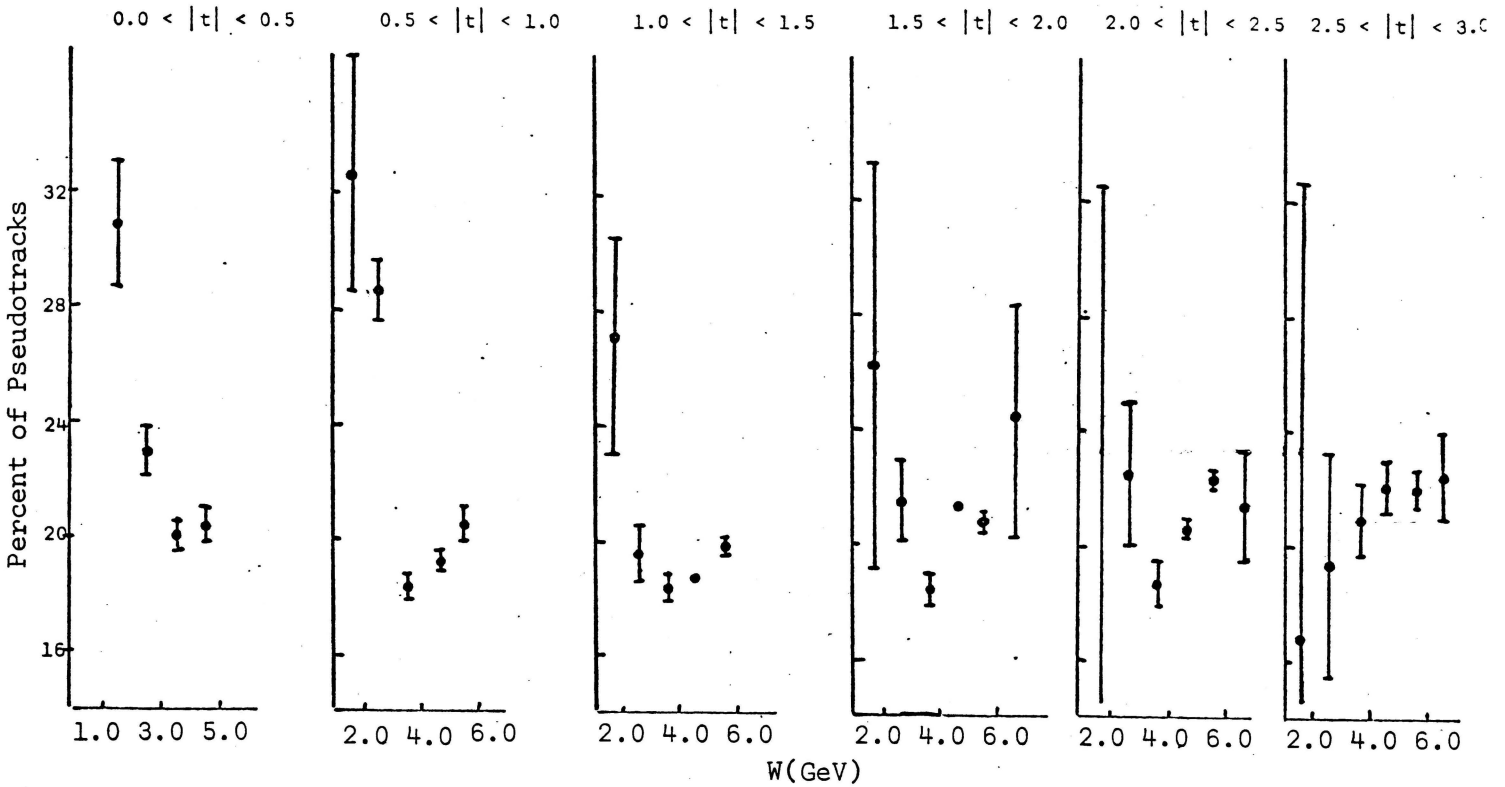

Figure 2A. Pseudotracks in 6 Prong Events in Each W-t Bin.

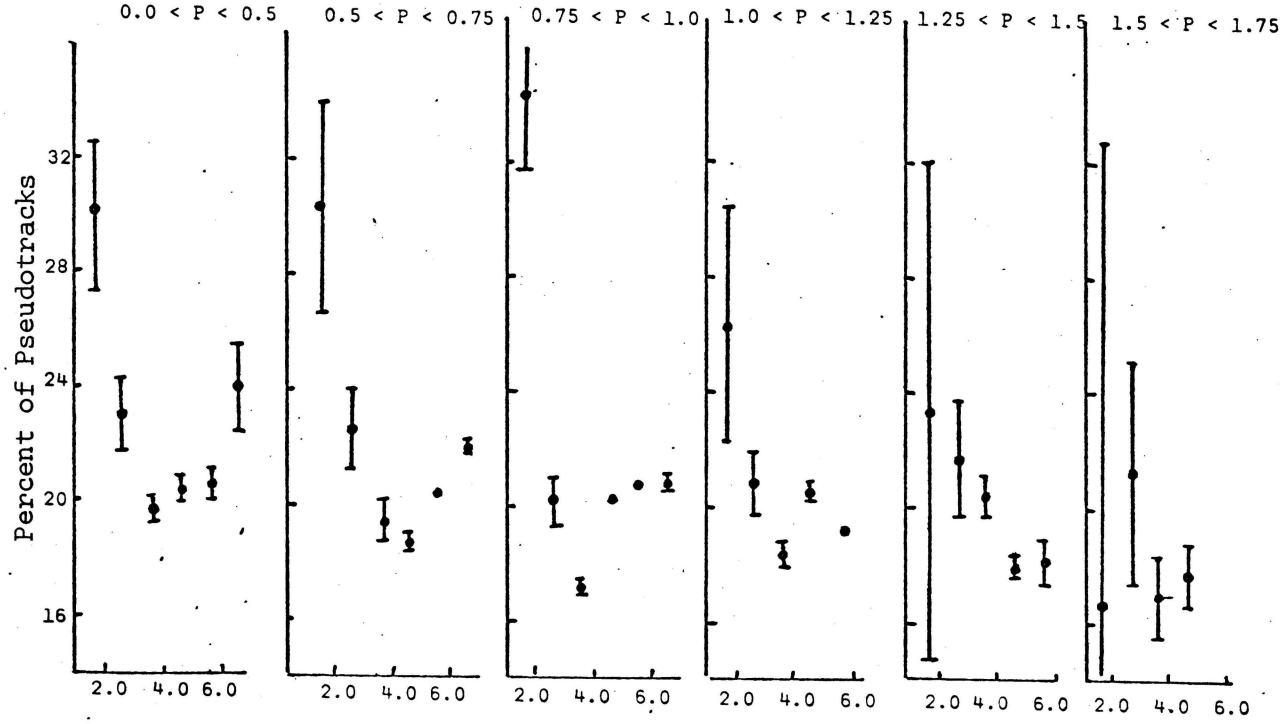

Figure 2B. Pseudotracks in 6 Prong Events in Each W-P Bin.

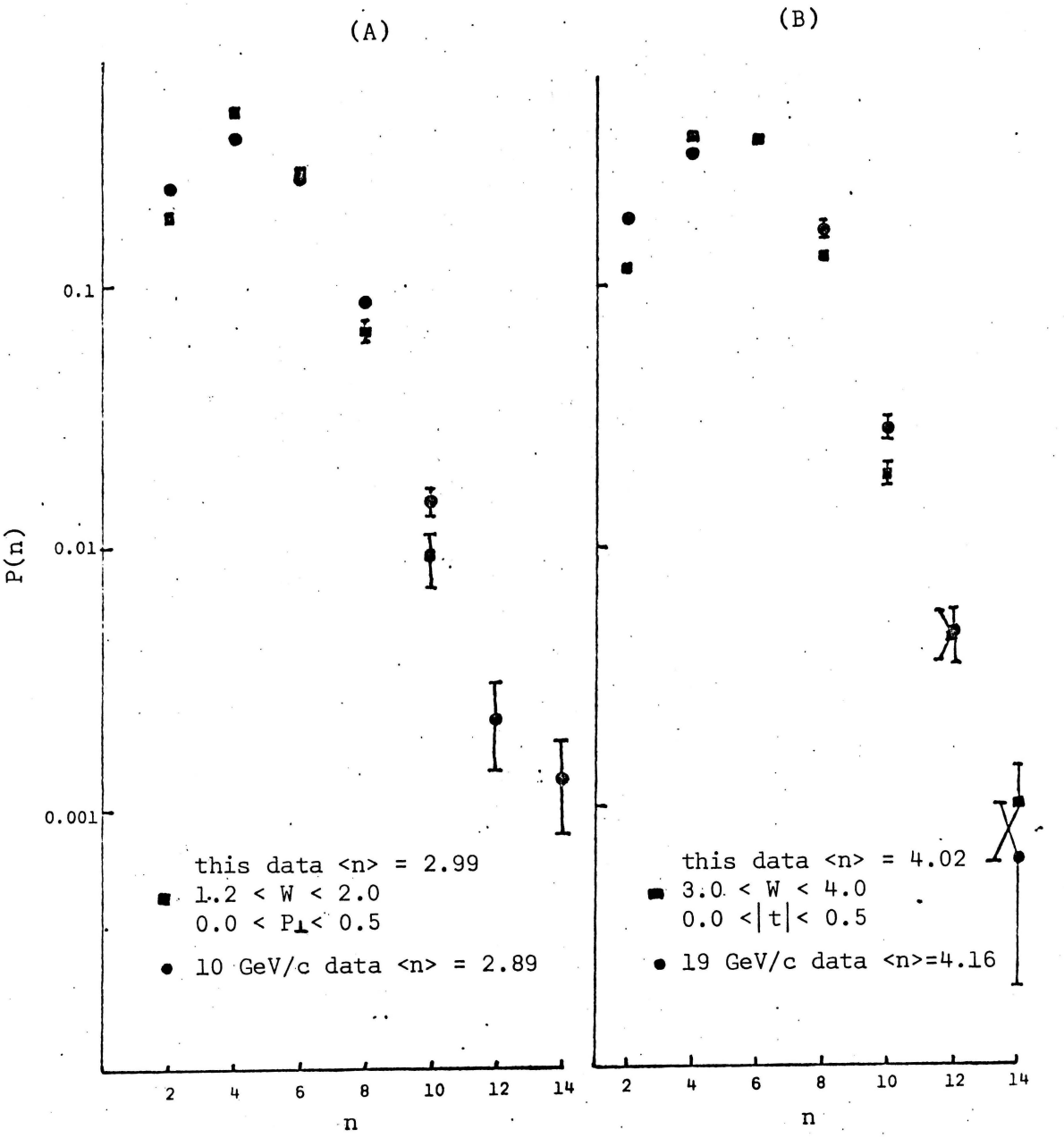

Figure 3. Some typical charge multiplicity distributions for the same <n>.

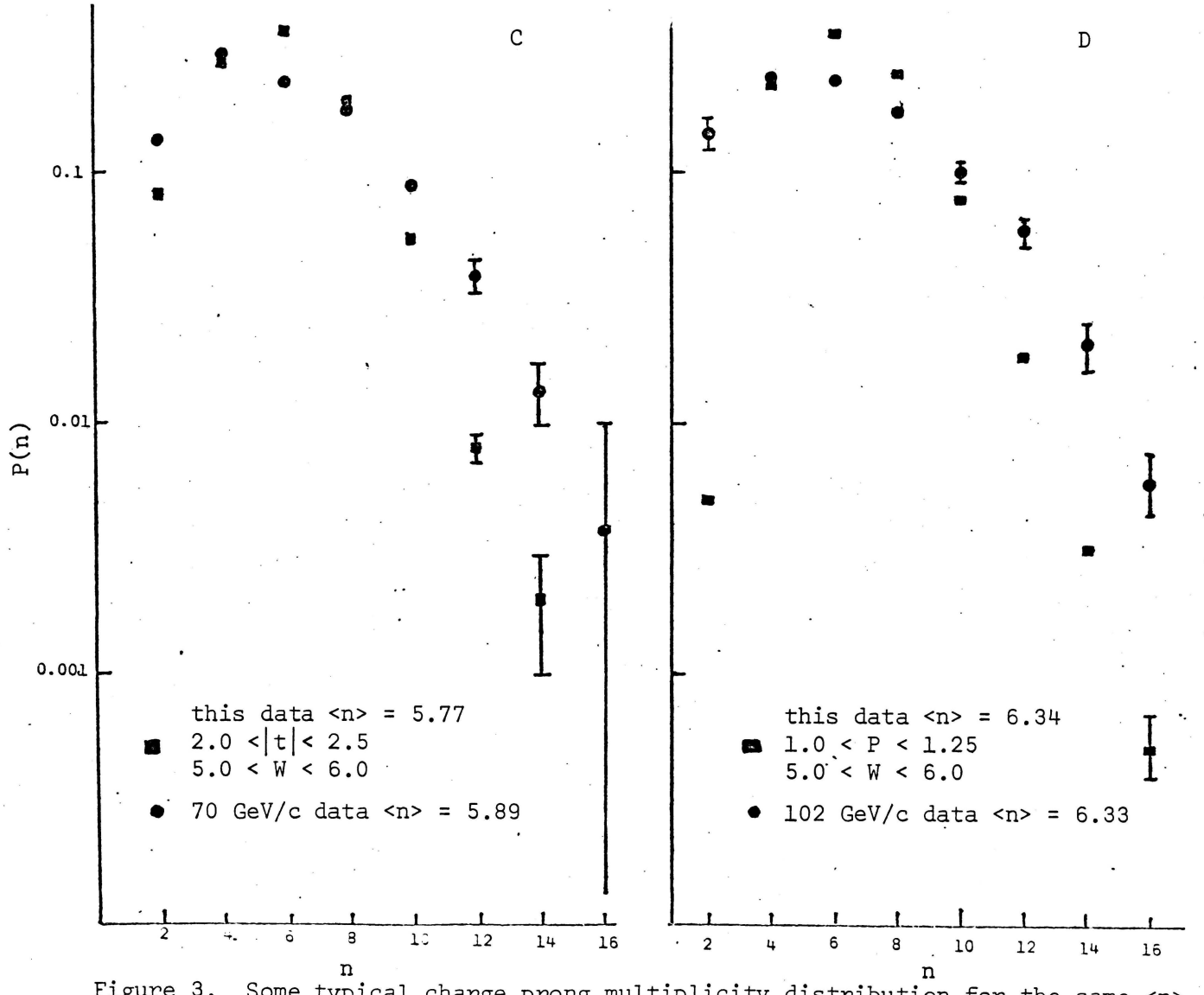

Figure 3. Some typical charge prong multiplicity distribution for the same <n>.

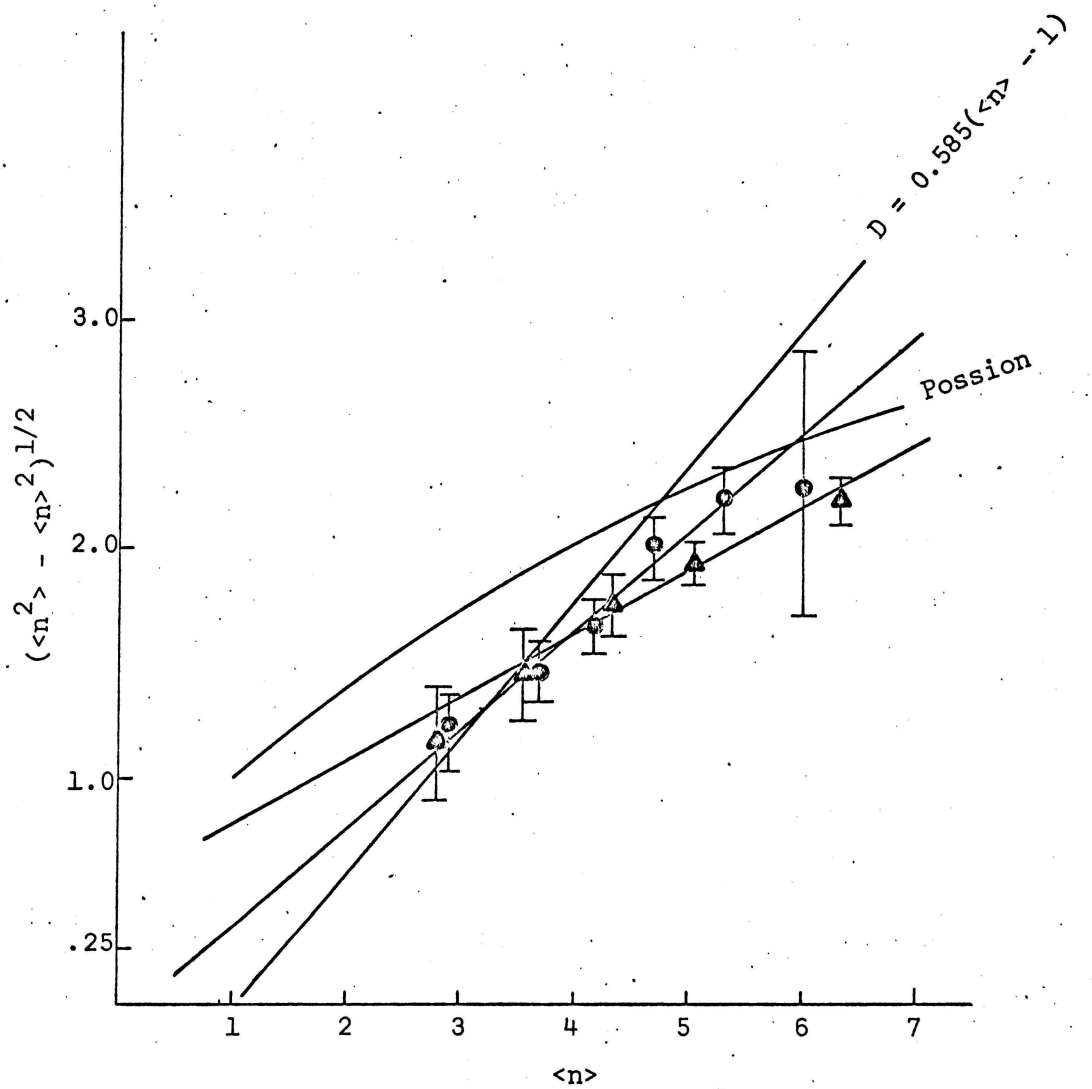

Figure 4. Plot of D vs. <n> for two W-P Bins. The curved line is the relation between <n> and D for Possion distributions.

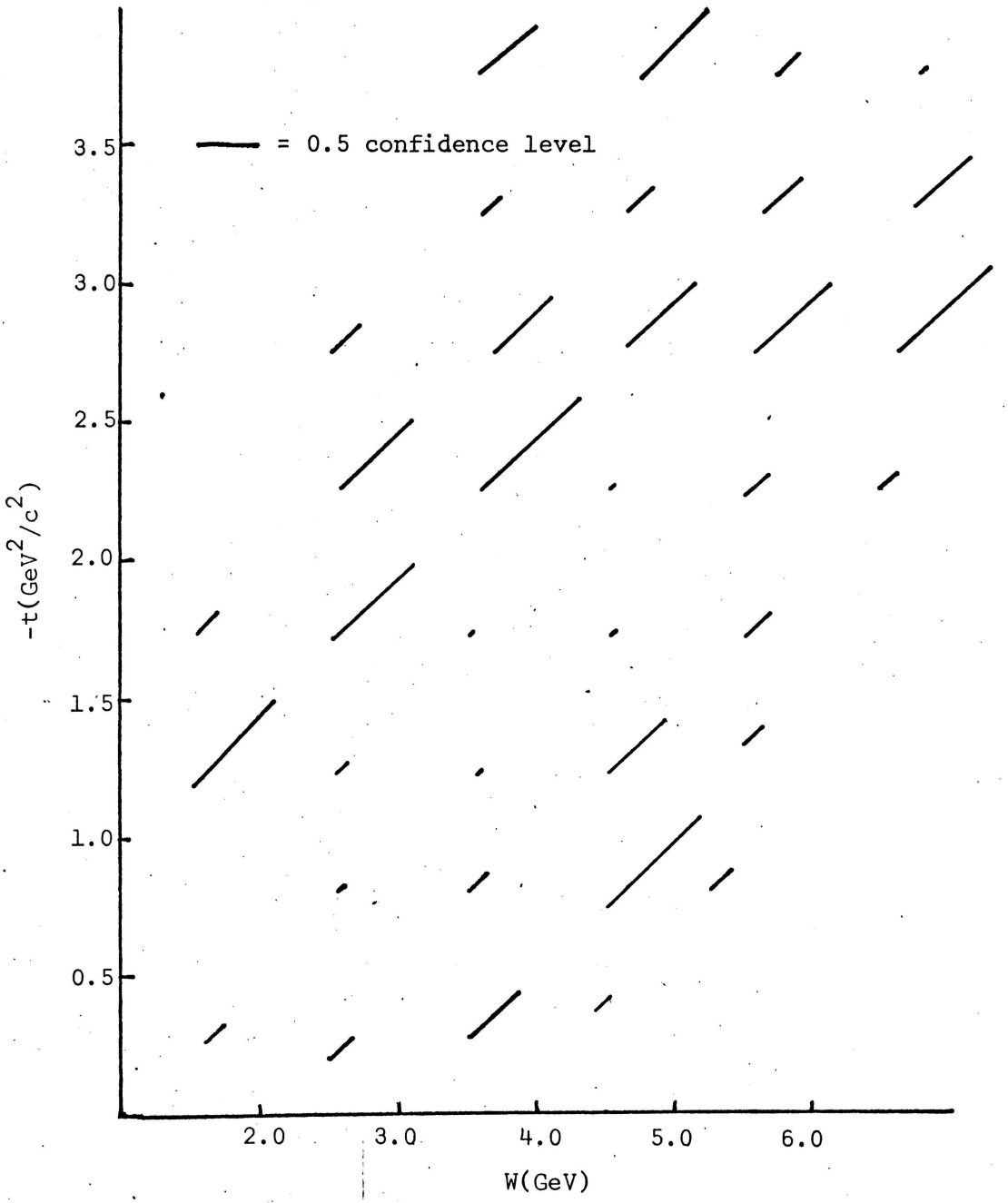

Figure 5A. Confidence level for fits of P(n,W,t) to $\exp(b_1x^3 + b_2x^2 + b_3x + b_4)$.

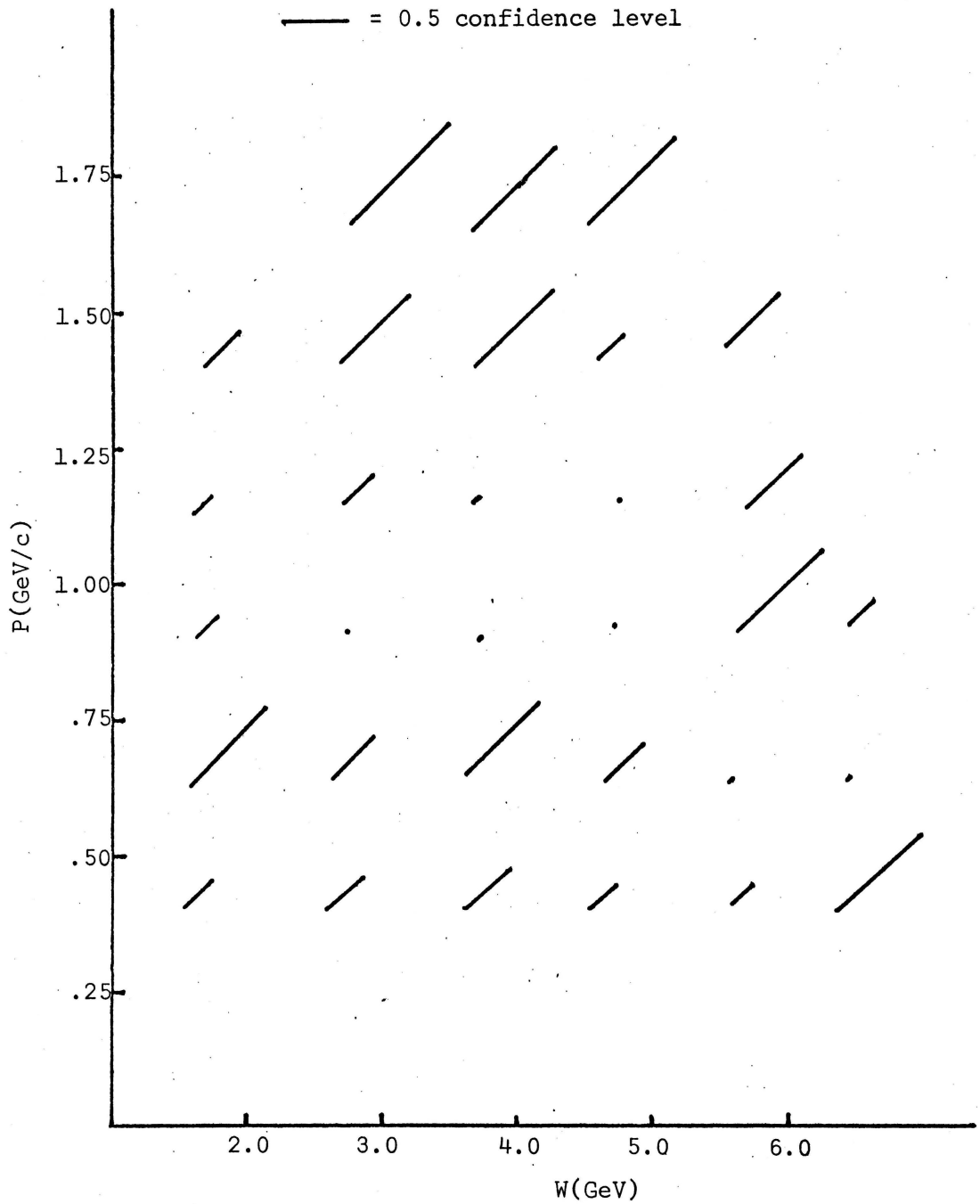

Figure 5B. Confidence level for fits of P(n,W,P) to $\exp(b_1x^3 + b_2x^2 + b_3x + b_4)$.

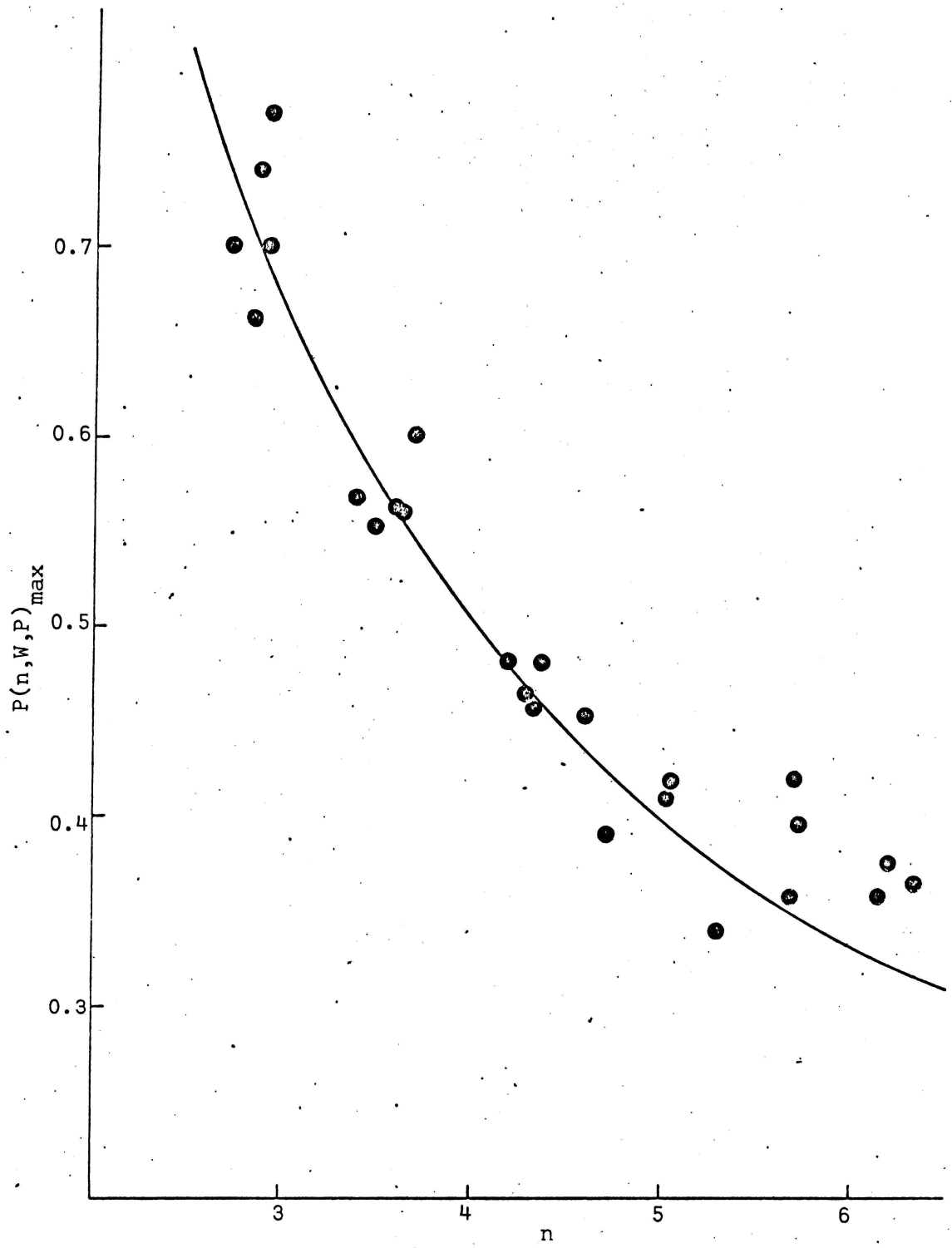

Figure 6. Plot of $P(n,W,P)$ vs. n. Curve shown is for the curve $P(n,W,P) = 2/n$.

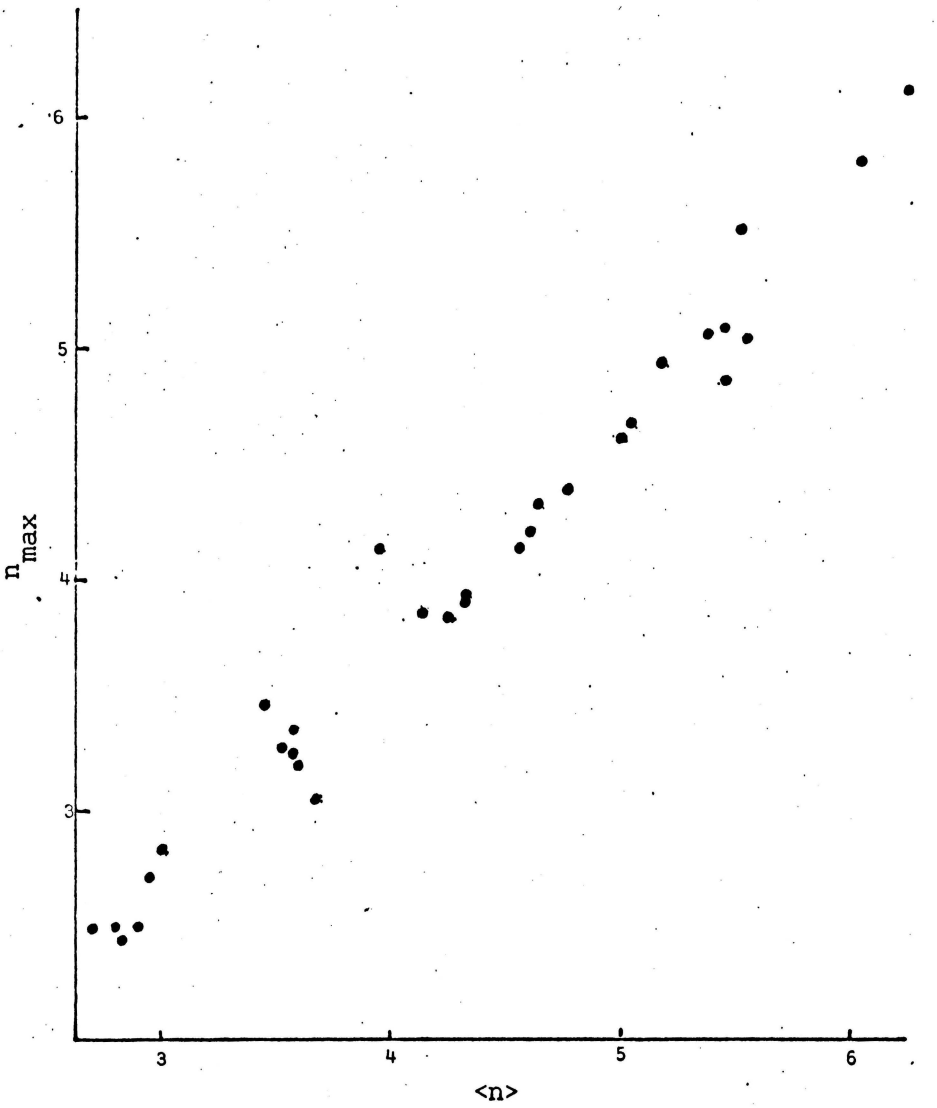

Figure 7. Plot of <n> vs. value of n,n_{max} for which P(n,W,t) is a maximum.

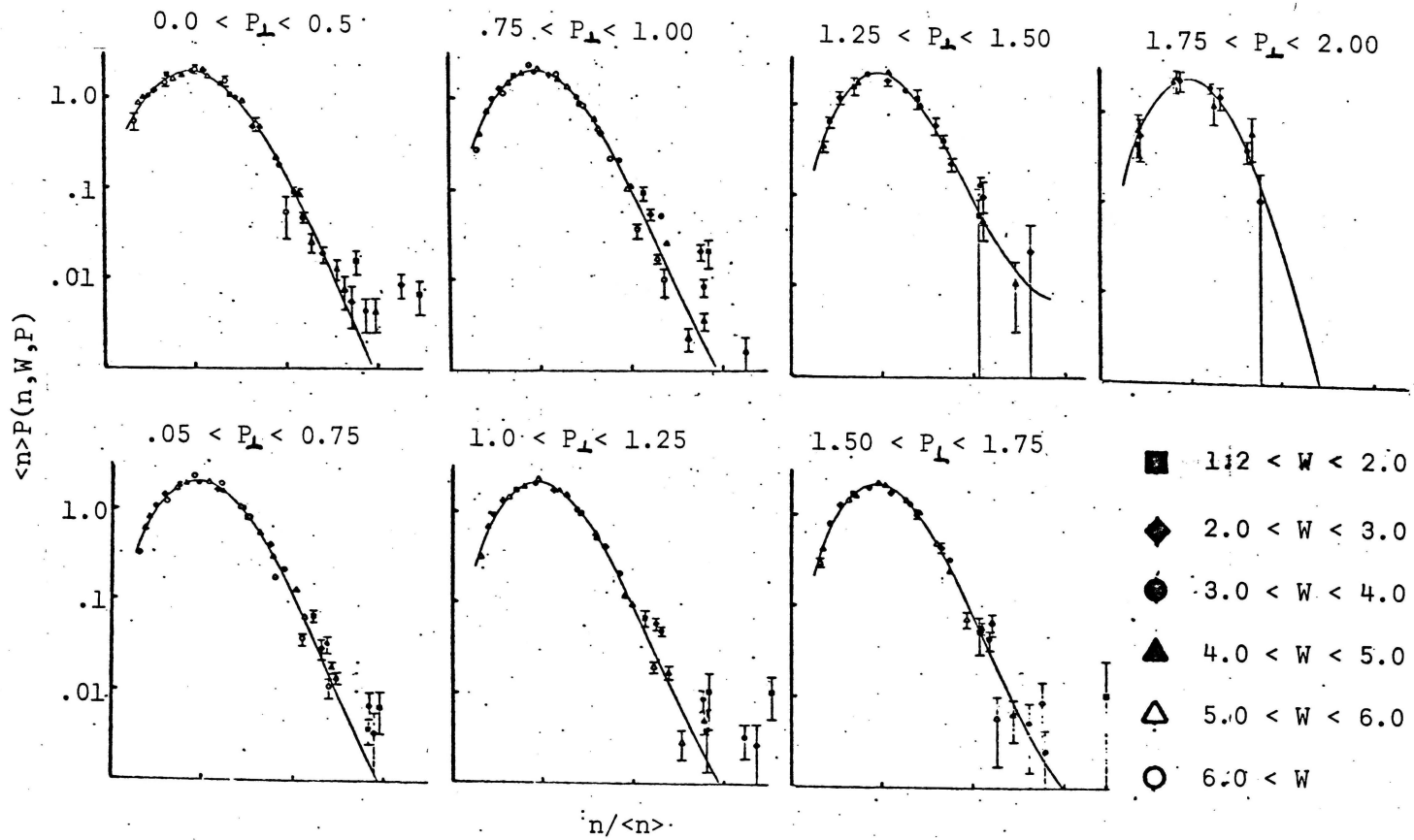

Figure 8A. Plots of <n>P(n,W,P) vs. n/<n>.

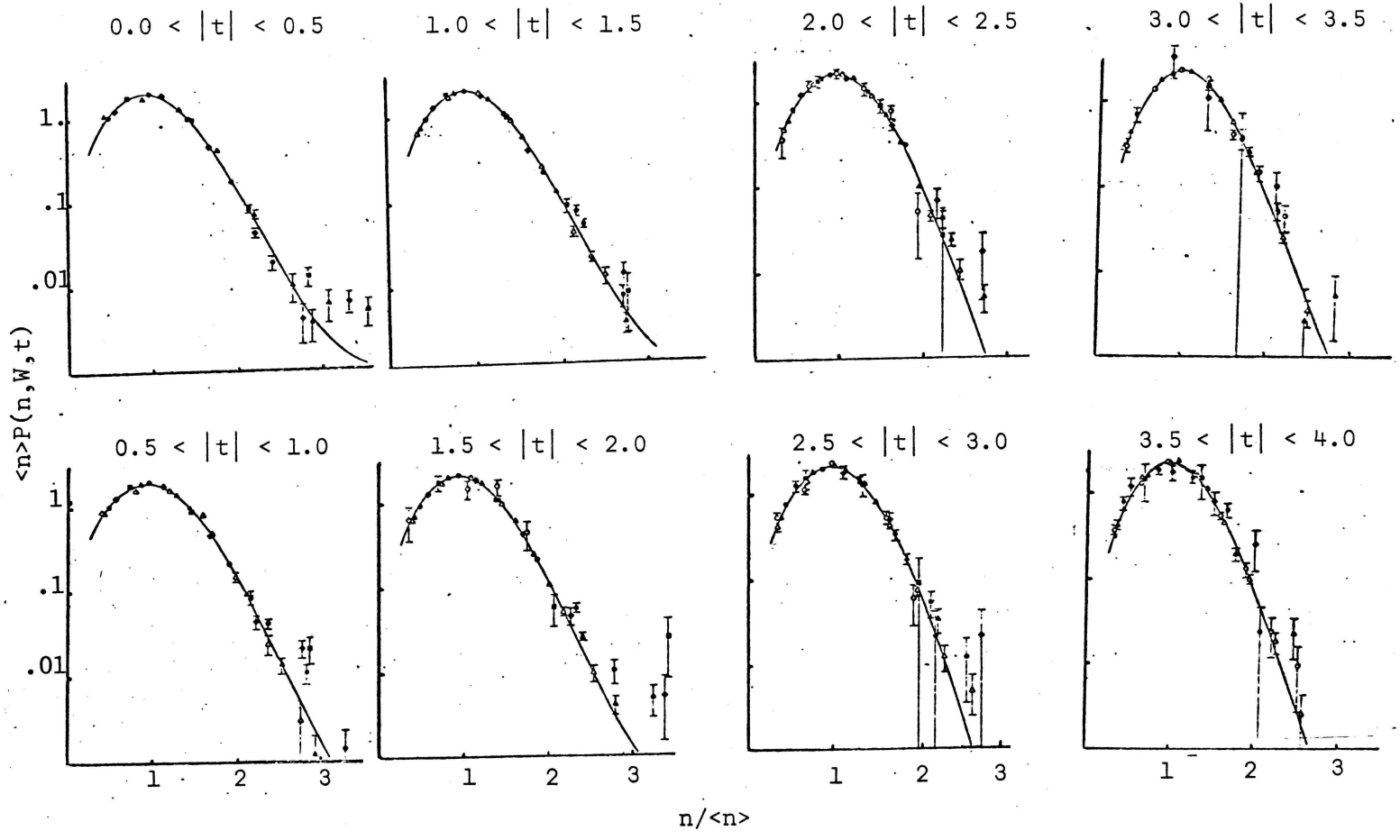

Figure 8B. Plots of <n>P(n,W,t) vs. n/<n> for each t bin.

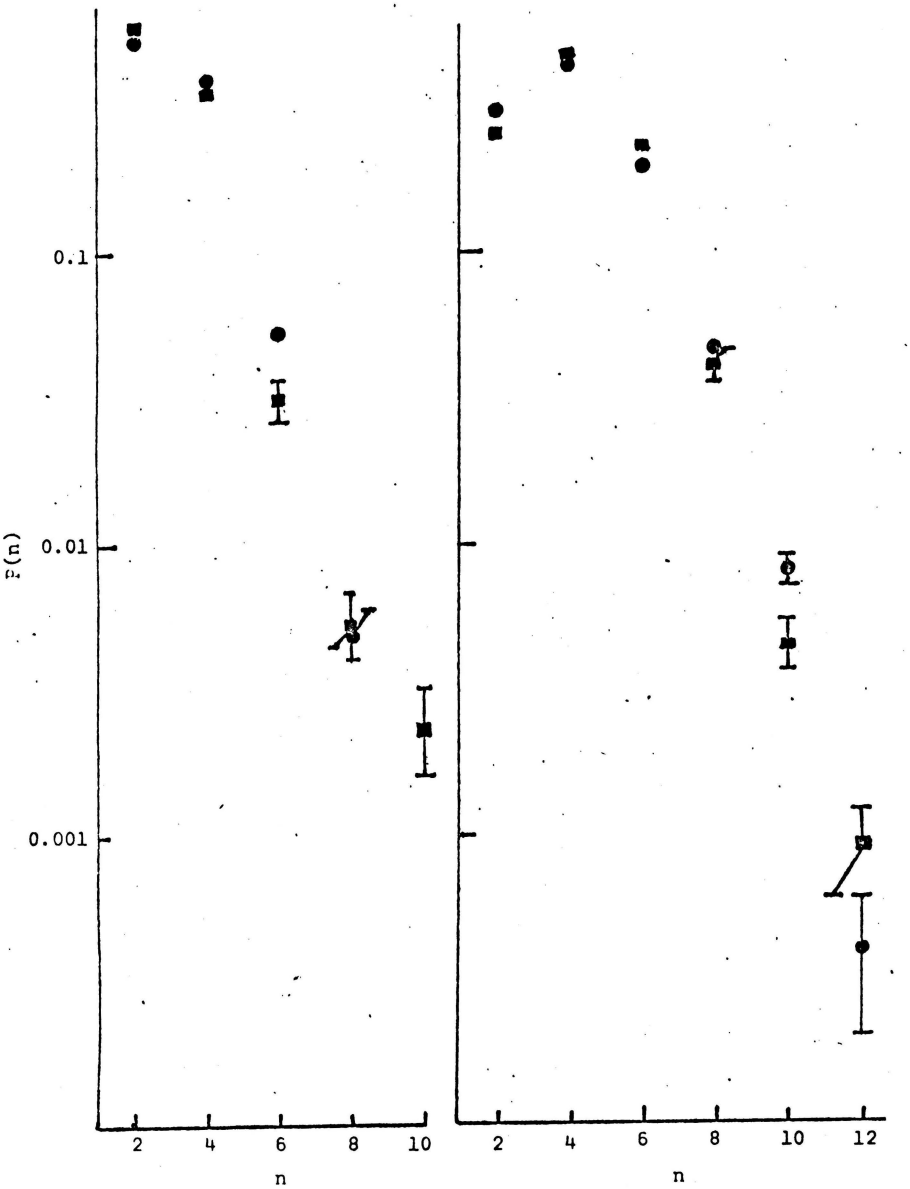

Figure 9. Comparison of two P(n,W,t) with the same <n>.

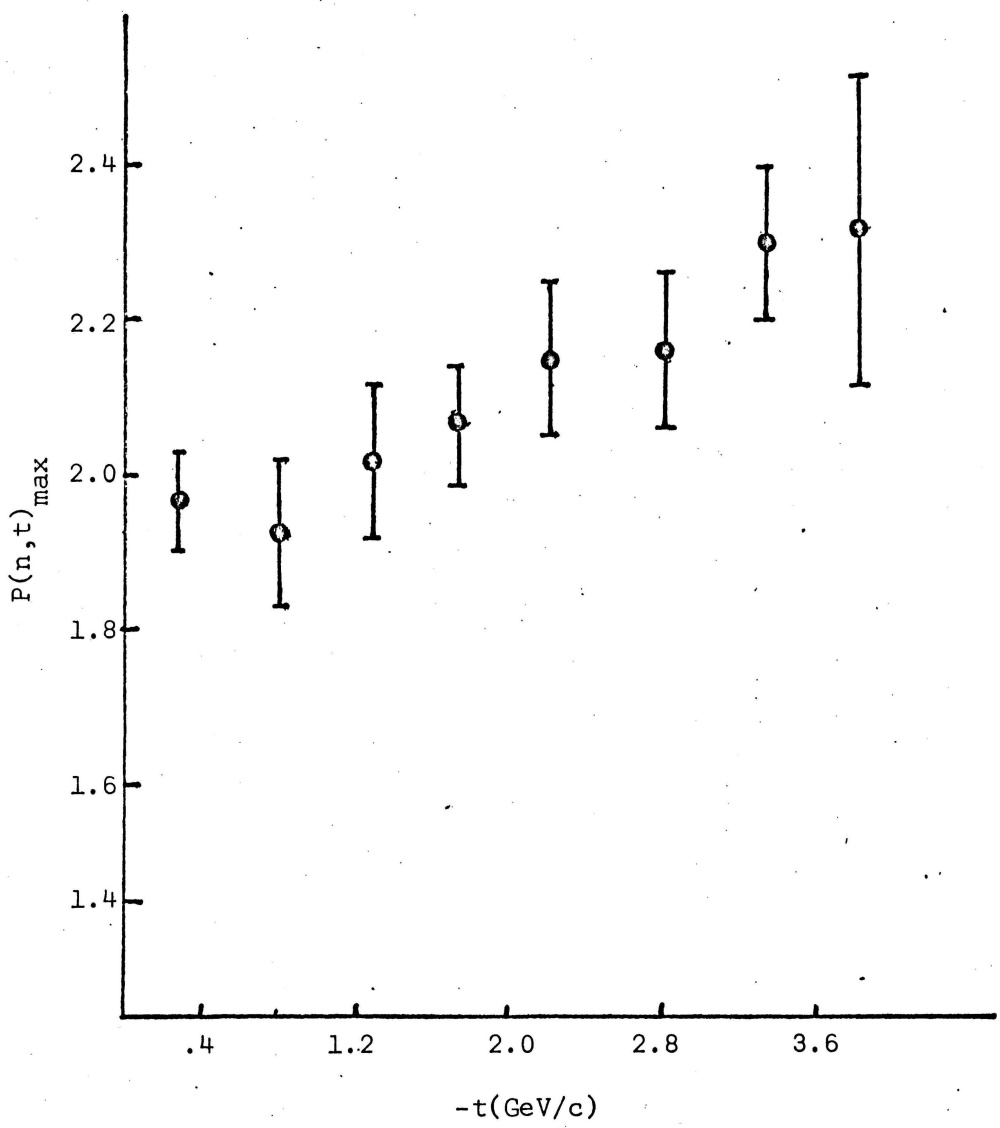

Figure 10. Plot of $P'(z_{max},t)$ vs t.

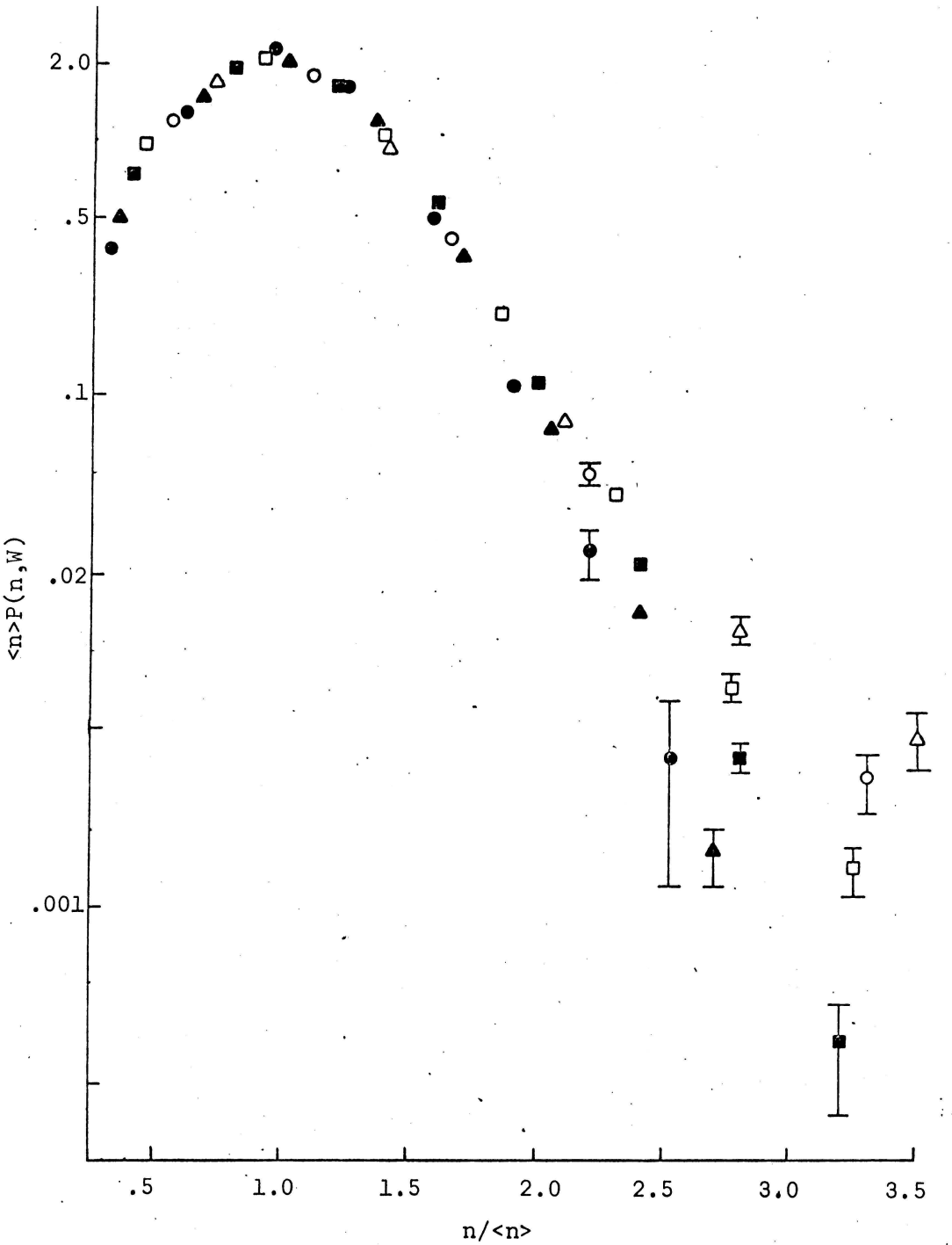

Figure 11. Plot of n/<n> vs. <n>P(n,W).

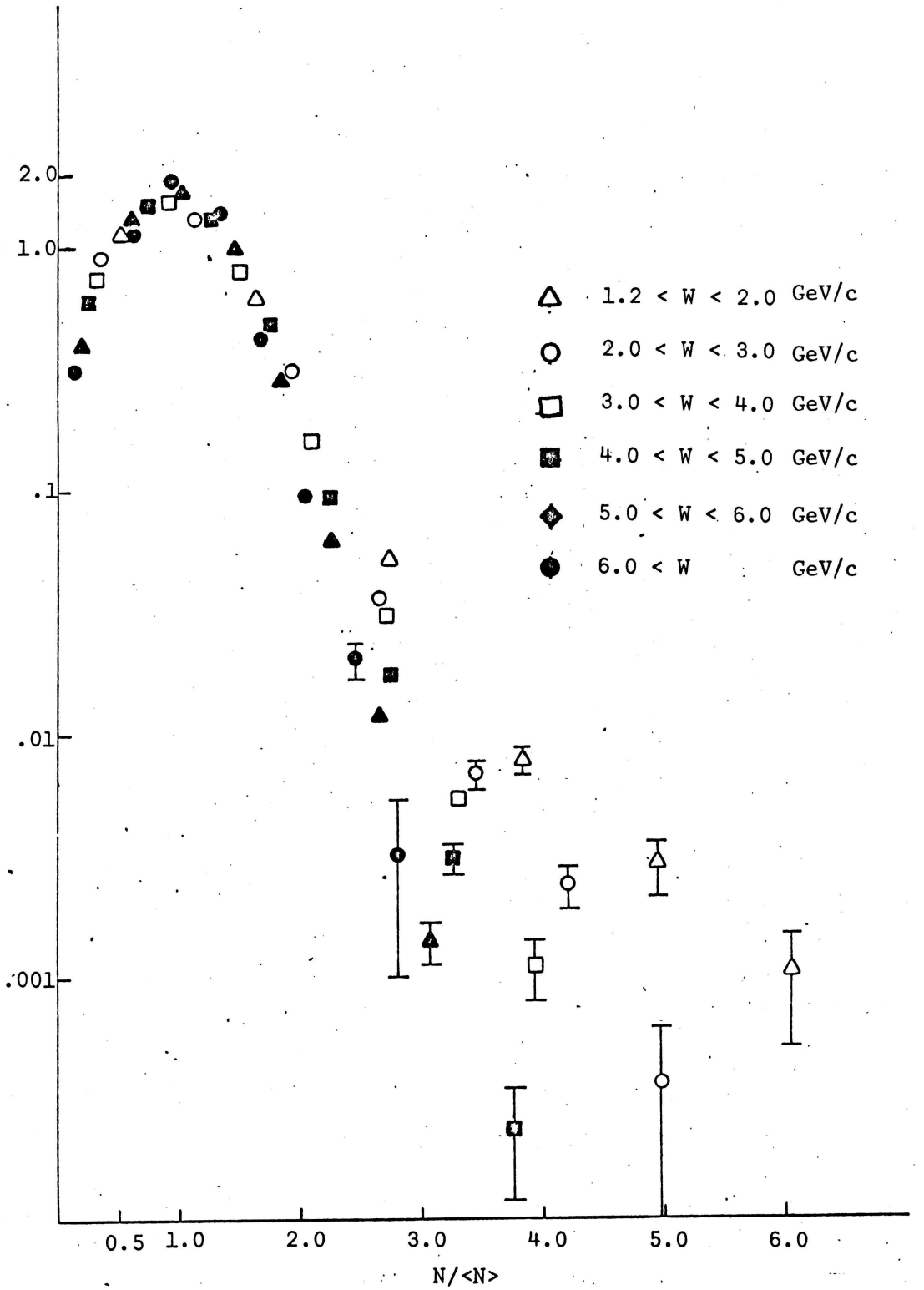

Figure 12. Plot of <N>P(N,W) vs. N/<N>.

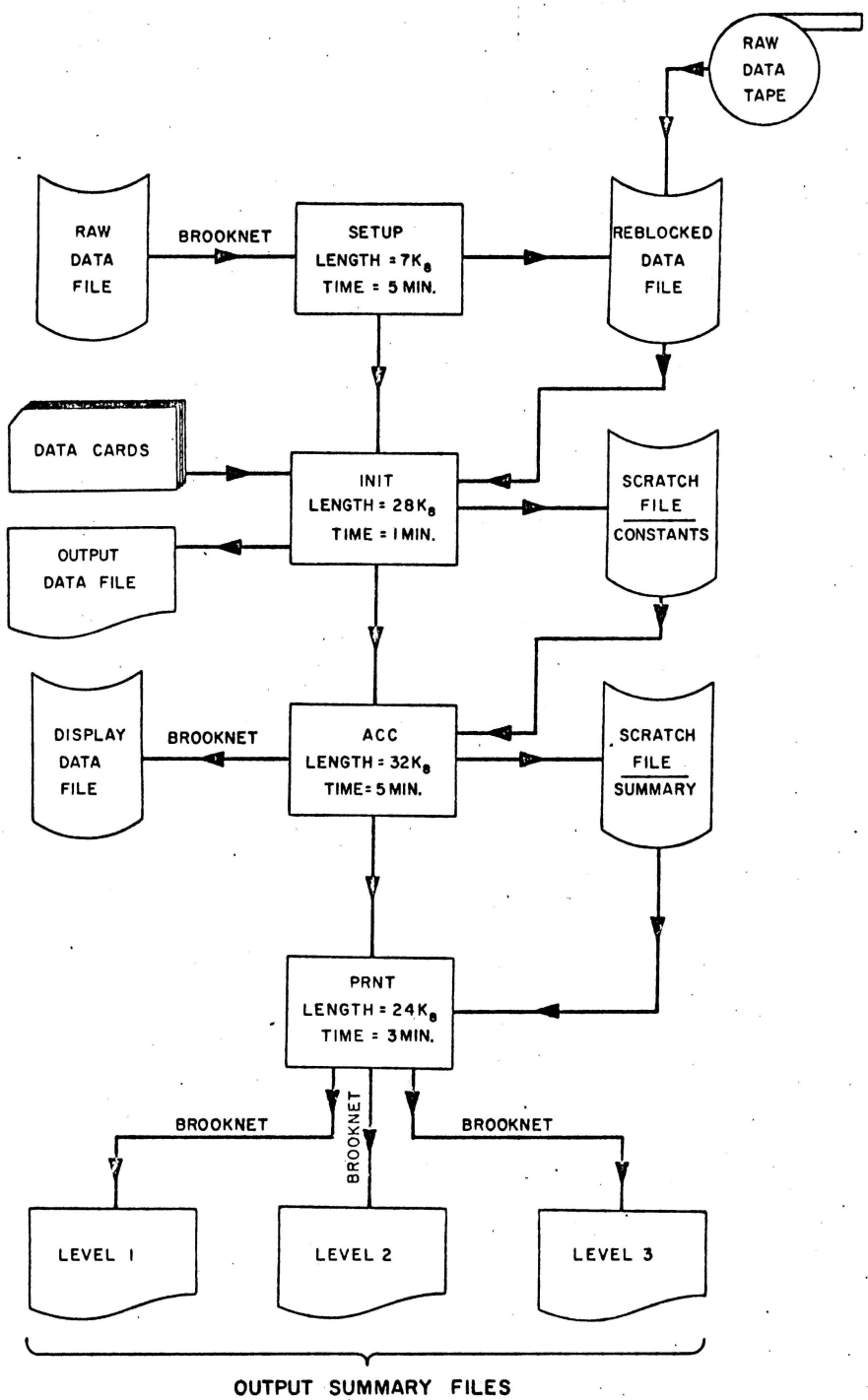

Figure 13. Flow Diagram for the ONLINE Program.

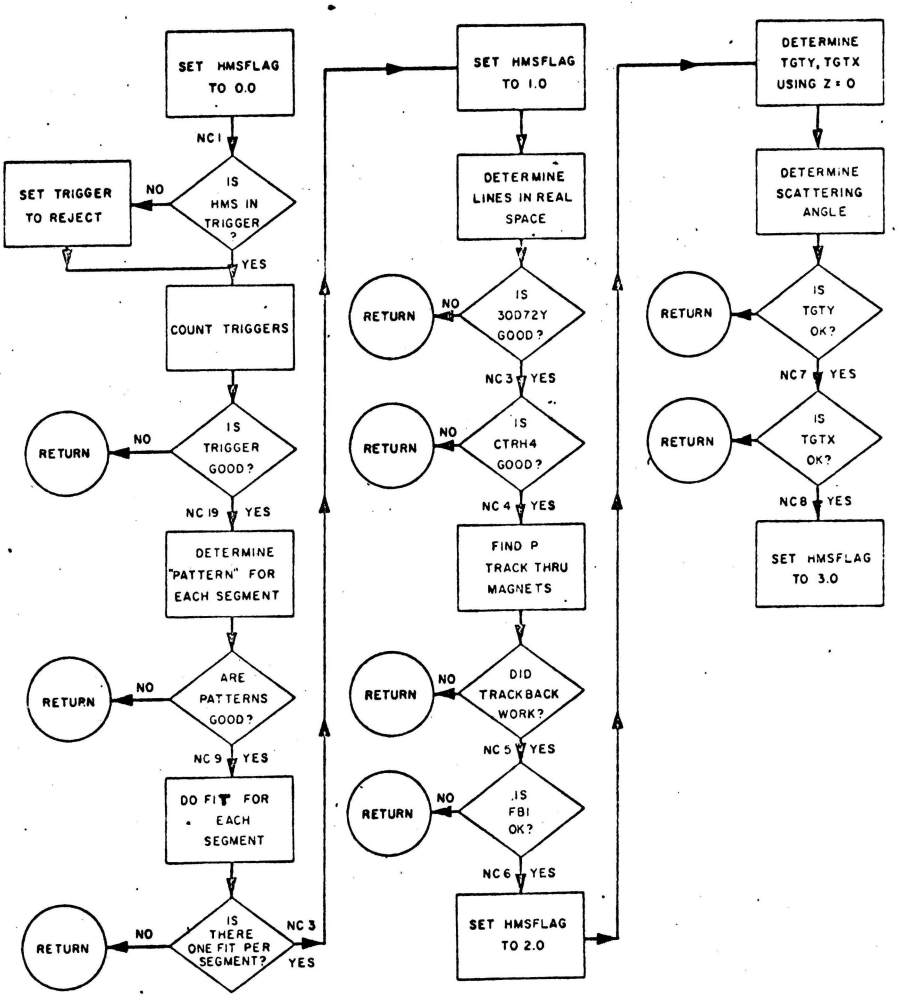

Figure 14. Flow Diagram for the HMS Driver Subprogram, HMSBOSS.

6600 ONLINE COVER SHEET FOR 396

RUN 463 TAPE R02430 MADE 21 OCLOCK ON 4/22/72 PROGRAM RAN AT 20.02.16. ON 04/25/72

HMS POSITION 3 LMS POSTION 9 TARGET F

MAGNET SETTINGS(KG)		FIELD USED(KG)	EFFECTIVE LENGTH(IN)
18D72	+12	,00	1,00
30D72	+12	12,26	79,38
48D48	+08	7,72	63,85
ARGO	-10	-9,35	31,22

RAW SCALERS

0 2934802 463 574423233882 0 35383689 0 30684455 0 28368319 0

RUN	BURSTS	R485/BURST	R2(UNSLVD)/BURST	INC PROTS(UNSLVD)/B	INC PROTS(SLVD)/B	INTERACTIONS(UNSLVD)/B
463	574	51129	7373413	616441	534572	49422

AV AGS ENERGY(GSSMTR)	EVENTS/SLAVED BEAM	AV TRIGGERS/BURST	SLAVE RATIO	R485/INC PROTS(UNSL)
28,44	8,1474 10**6	4,36	,87	,08

TOTAL INCDNT PROTONS	TOTAL INTERACTIONS	TOTAL CROSS SECTION(MB)	CONFUSION/EVENT	EXPECTED
353,837 10**6	28,368 10**6	93,688	,214	,040

2500 EVENTS ANALYZED WITH 0,00 PERCENT ILLEGAL, (0 = 0 0 0 0 0 0 0 0 0)

P-P	P-PI	PI-P	PI-PI	P-DSH	PI-DSH	DSH-P	DSH-PI	TOTAL
,12	,04	,04	0,00	39,20	22,36	27,84	10,20	100,00

PERCENT REJECTED, HIERARCHICAL ORDER

MODO FAIL	33,3	0,0	100,0	0,0	4,4	5,0	4,6	8,2	5,0
CONFUSION FLAG	0,0	0,0	0,0	0,0	19,2	20,4	21,7	20,0	20,2
HMS TRK RECON	0,0	0,0	0,0	0,0	16,3	18,3	0,0	0,0	13,5
HMS VERTEX CUT	33,3	0,0	0,0	0,0	38,5	30,1	0,0	0,0	21,9
LMS TRK RECON	0,0	0,0	0,0	0,0	0,0	0,0	14,2	13,3	5,3
LMS VERTEX CUT	33,3	0,0	0,0	0,0	0,0	0,0	46,8	32,9	16,4
TOF TROUBLE	0,0	0,0	0,0	0,0	0,0	0,0	,6	,4	,2
CRENC-TOF INCOMPT	0,0	0,0	0,0	0,0	0,0	0,0	0,0	,4	,0
HMS TRACK IN ARGO	0,0	100,0	0,0	0,0	,6	,4	0,0	0,0	,4
LMS TRACK IN ARGO	0,0	0,0	0,0	0,0	0,0	0,0	4,7	9,8	2,3
PERCNT SURVIVING	0,0	100,0	0,0	0,0	21,6	26,2	12,1	24,7	20,3
EVENTS SURVIVING	0	1	0	0	212	148	84	63	508
USING RIGHT PASS	0	1	0	0	212	148	59	88	508

TRIG CHANGES (6-5)= 0 (3-1)= 0 (4-2)= 0 (3-2)= 0 (1-2)= 1 (3-4)= 0 (7-8)= 32

PERCENT THAT FAILED THESE TESTS,

MODO FAIL	33,3	0,0	100,0	0,0	4,4	5,0	4,6	8,2	5,0
CONFUSION FLAG	0,0	0,0	0,0	0,0	20,0	22,0	22,7	22,0	21,4
HMS TRK RECON	33,3	0,0	0,0	0,0	23,0	25,0	0,0	0,0	23,7
HMS VERTEX CUT	66,7	0,0	100,0	0,0	72,1	66,0	0,0	0,0	69,9
LMS TRK RECON	33,3	0,0	0,0	0,0	0,0	0,0	15,5	19,6	19,6
LMS VERTEX CUT	66,7	0,0	0,0	0,0	0,0	0,0	82,6	65,5	77,8
TOF TROUBLE	0,0	0,0	0,0	0,0	0,0	0,0	1,4	,8	1,3
CRENC-TOF INCOMPT	0,0	0,0	0,0	0,0	0,0	0,0	0,0	,8	,2
HMS TRACK IN ARGO	100,0	100,0	100,0	0,0	72,6	66,7	0,0	0,0	70,7
LMS TRACK IN ARGO	100,0	100,0	100,0	0,0	0,0	0,0	90,4	81,2	88,0

Figure 15a. Sample ONLINE output - Cover Sheet.

6600 ONLINE COVER SHEET FOR HMS

RUN 463 TAPE 802430 MADE 21 OCLOCK ON 4/22/72 PROGRAM RAN AT 20.02.16, ON 04/22/72

		P-P	P-PI	PI-P	PI-PI	P-DSH	PI-DSH	DSH-P	DSH-PI
ANALYZED	1549	,19	,06	,06	0,00	63,27	36,41	0.00	0,00
PASSED	467	,21	,21	0,00	0,00	58,46	41,11	0.00	0,00

ANALYZED= 1549 MULT OK= 82,8 TRACKS IN ALL SEGMENTS= 76,3 MOMENTUM FOUND= 72,2 VERTEX GOOD= 30,1

SEGMENT	1	2	3	ALL 3
MULT.				
1111	48,93	53,26	81,02	39,06
0111	17,24	18,66	7,42	1,36
2111	11,68	10,65	5,55	,58
2211	5,75	4,97	,71	0,00
0211	3,55	2,13	,52	0,00
0011	2,97	3,16	,45	0,00
0000	,13	,13	,84	0,00
OTHER	9,75	7,04	3,49	,26

EFFICIENCIES	86,68	90,50	96,99	97,40	87,42	89,81	97,21	97,93	95,74	97,99	98,31	98 07			
FITS															
MEAN(FIT-MEAS)	-,005	,005	-,005	-,005	,005	-,005	,005	-,005	-,005	-,005	-,005	-,005			
FWHM(FIT-MEAS)	,040	,030	,040	,050	,050	,040	,050	,070	,040	,020	,030	,040			
CHISQ CUT(3-4)		3,00	3,00			3,00	3,00			3,00	3,00				
SIGMA USED		,012				,024				,012					
GOOD TRK(3-4-IL)	27,30	68,72	96,02		27,07	70,90	97,97		5,59	87,36	96,96		92,20		
CHAMBER OFFSETS		0,000	,006	-,022	0,000				0,000	-,004	-,037	0,000			
		0,000	-,002	,009	0,000										

CUTS	30D72Y	CTRH3	FBI(AT EXIT 30D72)	TGTY	TGTX
MIN(INPUT)	-3,00	783,62	-,40	-,40	-,10
MAX(INPUT)	3,00	787,17	,40	,40	,60
PCT. PASSED	99,41	99,07	94,92	97,32	42,40

AVG MM 0,000 ERROR 0,000 WIDTH 0,000 ERROR 0,000 MAX VALUE 1,185 NUMBER IN MAX BIN 0

Figure 15b. Sample ONLINE output - HMS Cover Sheet.

The vita has been removed from the scanned document

CHARGE PRONG MULTIPLICITY DISTRIBUTIONS IN PROTON-PROTON COLLISIONS AT 28.5 GeV/c

by

Thomas S. Clifford

(ABSTRACT)

Using the Multiparticle Argo Spectrometer System, we have measured the charge prong multiplicity distribution as a function of the kinematic variable of the fast recoil proton for 190,000 events in the reaction pp→p+ANYTHING at 28.5 GeV/c. We find the distributions to be similar to charge prong multiplicities for pp→ANYTHING at different energies. We have looked for a KNO type scaling in W, $P_{\perp}$ and t and find strong evidence only for scaling over W for a fixed range of t.

Finally, the scaled distributions, both total and associated, as a function of W are presented for comparison.